HHS Public Access

Author manuscript

Cell Rep. Author manuscript; available in PMC 2023 April 18.

Published in final edited form as:

Cell Rep. 2023 March 28; 42(3): 112203. doi:10.1016/j.celrep.2023.112203.

A Non-Hallucinogenic LSD analog with Therapeutic Potential for Mood Disorders

Vern Lewis[1,5], **Emma M. Bonniwell**[2,5], **Janelle K. Lanham**[2,5], **Abdi Ghaffari**[4], **Hooshmand Sheshbaradaran**[4], **Andrew B. Cao**[2], **Maggie M. Calkins**[2], **Mario Alberto Bautista-Carro**[1], **Emily Arsenault**[1], **Andre Telfer**[1], **Fatimeh-Frouh Taghavi-Abkuh**[1], **Nicholas J. Malcolm**[2], **Fatema El Sayegh**[1], **Alfonso Abizaid**[1], **Yasmin Schmid**[3], **Kathleen Morton**[3], **Adam L. Halberstadt**[3,6,7], **Argel Aguilar-Valles**[1,6,7], **John D. McCorvy**[2,6,7,8]

[1.]Department of Neuroscience, Carleton University, Ottawa, ON, K1S 5B6, Canada

[2.]Department of Cell Biology, Neurobiology and Anatomy, Medical College of Wisconsin, Milwaukee, WI, 53226, USA

[3.]Department of Psychiatry, University of California San Diego, La Jolla, CA, 92093, USA

[4.]BetterLife Pharma Inc., Vancouver, BC, V6H 1A6, Canada

[5.]Authors have contributed equally to the manuscript

[6.]Co-corresponding authors

[7.]Senior authors

[8.]Lead contact

Summary

Hallucinations limit the widespread therapeutic use of psychedelics as rapid-acting antidepressants. Here we profiled the non-hallucinogenic lysergic acid diethylamide (LSD) analog 2-bromo-LSD (2-Br-LSD) at >33 aminergic G protein-coupled receptors (GPCRs). 2-Br-LSD shows partial agonism at several aminergic GPCRs, including 5-HT_{2A} and does not induce the head-twitch response (HTR) in mice, supporting its classification as a non-hallucinogenic 5-HT_{2A} partial agonist. Unlike LSD, 2-Br-LSD lacks 5-HT_{2B} agonism, an effect linked to cardiac valvulopathy. Additionally, 2-Br-LSD produces weak 5-HT_{2A} β-arrestin recruitment and internalization *in vitro* and does not induce tolerance *in vivo* after repeated administration. In cultured rat cortical neurons, 2-Br-LSD induces dendritogenesis and spinogenesis, and increases active coping behaviour in mice, an effect blocked by the 5-HT_{2A}-selective antagonist volinaserin (M100,907). 2-Br-LSD also reverses the behavioral effects of chronic stress. Overall, 2-Br-LSD

corresponding authors: Adam L. Halberstadt: ahalberstadt@health.ucsd.edu, Argel Aguilar-Valles: argel.aguilavalles@carleton.ca, John D. McCorvy: jmccorvy@mcw.edu.

Author Contributions

A.G., H.S., A.L.H., A.A.V., and J.D.M. conceived of the project. J.D.M. supervised the GPCR experiments and were conducted by E.M.B., J.K.L., N.J.M., A.B.C., and M.M.C. Constructs were generated by J.K.L., M.M.C. and J.D.M. HTR experiments were conducted by K.M. and Y.S. and supervised by A.L.H. A.A.V. supervised the *in vivo* experiments and were conducted by V.L., E.A., F.F.T.A., and F.E.S. Neuronal culture experiments conducted at Carleton University, were supervised by A.A.V. and run by V.L. & M.A.B.C. Video analysis was supervised by A.A. and conducted by A.T. All authors provided comments on the manuscript.

Declaration of Interests

A.G. and H.S. are employees of BetterLife Pharma Inc.

has an improved pharmacological profile compared to LSD and may have profound therapeutic value for mood disorders and other indications.

Introduction

Current pharmacotherapies for major depressive disorder (MDD) and anxiety disorders, which are often comorbid[1,2], have drawbacks including delayed therapeutic onset, the need for chronic dosing, and large numbers of treatment-resistant patients[3,4]. Recently, there has been growing interest in psychedelics as treatment for a range of psychiatric disorders[5,6]. Psychedelics such as psilocybin, *N,N*-dimethyltryptamine (DMT), and (+)-lysergic acid diethylamide (LSD) can induce mystical states and profound alterations of consciousness, effects that are largely mediated by serotonin 2A (5-HT_{2A}) receptor activation[7,8]. In multiple double-blind, placebo-controlled trials, psilocybin, DMT, and LSD produced long-lasting reductions in depression and anxiety after only one or two doses[9–13]. However, the therapeutic use of psychedelics has limitations, including their intense hallucinogenic effects, which require close clinical supervision, and anxiety and confusion in some patients[14].

The degree to which the therapeutic effects of serotonergic psychedelics are linked to their subjective effects is not entirely clear. In several clinical trials, the level of symptom reduction produced by psilocybin was significantly correlated with metrics of drug-induced psychedelic phenomenology[15–17]. Thus, it has been proposed that the subjective effects of psychedelics are required for their therapeutic effects[18,19]. However, it may be possible to decouple the hallucinogenic effects of psychedelic drugs from their therapeutic effects[18]. The intensity of the psychedelic response induced by psilocybin is closely related to level of 5-HT_{2A} occupation[20,21], and this correlation could reflect a relationship between therapeutic response and target engagement. Furthermore, the pharmacological mechanism for antidepressant effects of psilocybin has not been characterized and may include other receptors[22].

An attractive hypothesis for antidepressant effects of psychedelics involves rapid induction of structural and functional neural plasticity and the reversal of neuronal atrophy in cortical regions[23–25]. Prefrontal pyramidal neurons exert top-down control over activity in regions involved in emotional processing, motivation, and reward, and atrophy of the spines and dendrites of pyramidal neurons could contribute to depression symptomology[26]. Preclinical models show that some psychedelic analogs do not produce behavioral effects associated with hallucinogenic effects but retain the ability to promote cortical neuritogenesis, similar to established antidepressant drugs[27].

Lysergic acid derivatives were the focus of intense research during the 1940s and 1950s. LSD was first synthesized by Dr. Albert Hofmann in 1938[28] and was investigated as a potential treatment for an extensive range of disorders[29]. Hofmann also synthesized (+)-2-bromolysergic acid diethylamide (2-Br-LSD, BOL-148; Fig. 1A), which did not induce hallucinogenic effects in humans[30,31]. Similar to LSD and psilocybin[32], 2-Br-LSD recently showed efficacy against cluster headaches[31], which is surprising because 2-Br-LSD was initially described as a 5-HT_{2A} antagonist[33] and could block the psychological response to

LSD[34]. Based on those findings, the possibility exists that 2-Br-LSD may also mimic some of LSD's anti-depressant and anxiolytic effects. Therefore, this study aimed to investigate the pharmacological profile of 2-Br-LSD, its psychedelic-like effects, and the potential for mood disorders treatment.

Results

Profiling 2-Br-LSD Across the Serotonergic and Amingeric GPCRome

Ergolines like LSD have a pronounced aminergic GPCR polypharmacology[35,36], making it necessary to interrogate 2-Br-LSD at many targets. Importantly, GPCR functional efficacy needs interrogation because traditional radioligand binding assays (i.e., K_i determinations) may not assess agonist molecular efficacy accurately[37]. Therefore, we performed a pan-aminergic-wide GPCR functional screening campaign using a G protein dissociation BRET-based assay platform[38] optimized for 33 human aminergic GPCRs (including serotonin, dopamine, adrenergic, histamine, and muscarinic subtypes; Fig. 1B and Table S1). We screened 2-Br-LSD and LSD in parallel at each of the 33 aminergic GPCR subtypes measuring select canonical G protein dissociation activity at conditions necessary for full receptor occupancy (37°C degrees/60 minutes, see Supporting Info), which is critical to offset LSD's slow binding kinetics[39].

Next, we ranked the top GPCR targets for 2-Br-LSD and LSD by calculating their relative activity (log E_{MAX}/EC_{50}) using the endogenous control standard and plotted a heat map of activities (Fig. 1C). Calculated potency parameters (EC_{50} and K_B estimates; Table S2) at select aminergic GPCRs were similar to affinity (K_i) values determined in radioligand binding studies (Table S3).

Interestingly, all five 5-HT_1 subtypes are within the top 10 targets of 2-Br-LSD, including the known anti-migraine drug targets 5-$HT_{1B/1D/1F}$[40] (Fig. 1D, Table S2). In fact, 2-Br-LSD demonstrated potent pan-agonism at all 5-HT_1 $G_{i/o}$-coupled receptor subtypes with similar G protein efficacies as LSD (Fig. S1A). At the other $G_{i/o}$-coupled serotonin GPCR, 5-HT_{5A}, however, 2-Br-LSD was a potent antagonist (K_B = 4.14 nM; Table S2) whereas LSD shows partial agonism.

Within the top ten targets, 2-Br-LSD and LSD demonstrated sub-nanomolar partial agonism at 5-HT_6 (EC_{50} = 0.35 and 0.13 nM, respectively, Fig. 1D), which is an emerging target for cognitive deficits[41]. At other G_s-coupled serotonin GPCRs, both LSD and 2-Br-LSD lack potent agonist or antagonist activity at 5-HT_4. At the 5-HT_{7a} subtype, however, 2-Br-LSD and LSD act as antagonists (Table S2) and both exhibit potent inverse agonism in a cAMP accumulation assay (EC_{50} = 5.1 and 17.3 nM, respectively; Fig. S1B).

Two dopamine receptors, D_2 and D_4, were also within the top 10 targets activated by 2-Br-LSD (EC_{50} = 0.35 and 1.2 nM, respectively; Fig. 1C–D, Fig. S2A, Table S2). At the D_3 subtype, however, 2-Br-LSD is a weaker partial agonist (E_{MAX} = 32% relative to dopamine) compared to LSD (E_{MAX} = 75%). Interestingly, 2-Br-LSD lacks strong agonism at $D_{1/5}$ subtypes, whereas LSD demonstrates agonist activity as previously reported[42] (Fig S2A, Table S2).

Surprisingly, 5-HT_{2A} and 5-HT_{2C} were at the bottom of the top 10 ranking list for 2-Br-LSD (Fig. 1D). At 5-HT_{2A}, 2-Br-LSD demonstrated Gq partial agonism (EC_{50} = 0.81 nM; E_{MAX} = 59.8%), whereas LSD is almost a full agonist at this receptor (EC_{50} = 0.35 nM; E_{MAX} = 91.5%). At 5-HT_{2C}, LSD is almost a full agonist, whereas 2-Br-LSD exhibits weaker Gq partial agonism (E_{MAX} = 45.8%). Furthermore, we confirmed many of the top 10 GPCR activities in orthologous assays measuring G protein-dependent second messenger assays (Fig. S1B).

At the remaining aminergic GPCRs, LSD and 2-Br-LSD show weaker agonist activity in general (Fig. S2B–E). At adrenergic GPCR subtypes, 2-Br-LSD displayed antagonistic activity at α_{1A}, α_{1B}, β_1 and β_2 (K_B=43, 38, 113, 47 nM, respectively, Table S2). Interestingly, differences between LSD and 2-Br-LSD were measured at α_{2A} and α_{2B}, where LSD shows partial agonism (E_{MAX} = 65% and 62% respectively; Table S2), and 2-Br-LSD instead antagonizes these receptor subtypes (K_B = 12 and 79 nM, respectively). By contrast, LSD and 2-Br-LSD both show partial agonism at the α_{2C} subtype (E_{MAX} = 80.2% and 40.5%, respectively; Table S2), but LSD is more efficacious and potent than 2-Br-LSD (EC_{50} = 0.56 and 10.4 nM, respectively). At histaminergic receptors, weak partial agonism of 2-Br-LSD was detected at H_2 that was only slightly greater than LSD. Importantly, neither 2-Br-LSD nor LSD possessed weak agonism or antagonism at the rest of the histamine and muscarinic GPCRs (Table S2). In summary, LSD exhibited agonist activity at 20 of 33 aminergic GPCR targets tested, but 2-Br-LSD was only active as an agonist at 14 of these GPCRs; notably, 10 of the 14 were serotonin GPCRs.

2-Br-LSD is a 5-HT_{2A} partial agonist and competitive partial antagonist

Activation of the 5-HT_{2A} receptor is a primary mediator of the psychedelic state and is responsible for the hallucinogenic effects of LSD[43,44]. While LSD acts as a highly efficacious Gq-agonist at 5-HT_{2A}, 2-Br-LSD produces only partial 5-HT_{2A} activation (E_{MAX} = 59.8%) but maintains high potency (EC_{50} = 0.81 nM; Table S2) similar to LSD. Partial agonists can also act as partial antagonists, given the basal levels of endogenous neurotransmitters in the brain[45], as noted for 5-HT_{2A} receptors[46]. Therefore, to assess partial antagonism of the receptor, 2-Br-LSD was tested as an antagonist in 5-HT_{2A} Gq dissociation and β-arrestin2 recruitment assays (Fig. 2A–B), where 5-HT and 2-Br-LSD were added simultaneously and incubated for 60 minutes to detect partial inhibition. Here, 2-Br-LSD potently and partially antagonized 5-HT_{2A} Gq and β-arrestin2 agonism by 5-HT (K_B = 0.18 and 0.07 nM, respectively; Table S2).

2-Br-LSD pharmacokinetics in plasma and brain

The pharmacokinetics of 2-Br-LSD were evaluated in mice to confirm bioavailability and brain penetrance (Fig. 2C, Table S4, Fig. S3A–C). After intraperitoneal administration (IP), plasma levels of 2-Br-LSD, quantified using LSD-d_3 as an internal standard, increased in a dose- and time-dependent manner. 2-Br-LSD was detected in plasma 10 min post-injection for all mice (Fig. S3B, C), with a time to maximum concentration (T_{max}) of 0.2 h, except for the male mice treated with 0.75 mg/kg (T_{max} = 0.5 h). Plasma concentrations were 2–5x higher in the male compared to the female mice; for example, the mean maximum plasma concentration (C_{max}) in mice treated with 6.75 mg/kg 2-Br-LSD was 1558.74 ng/mL (3.9

μM) in the males and 826.06 ng/mL (2.1 μM) in the females. As was the case for the C_{max}, the mean terminal half-life ($T_{1/2}$) was dependent on sex and dose, with a range of 1.2–1.4 h for the male mice and 0.9–2.6 h for the females. 2-Br-LSD rapidly crossed the blood-brain barrier with a mean T_{max} of 0.17 h in both male (Fig. 2C) and female mice (Fig. S3A). The mean $T_{1/2}$ of 2-Br-LSD in the brain ranged from 0.7–1.0 h for the males and 0.4–1.3 h for females (Table S4). The level of 2-Br-LSD in the brain was below the lower limit of detection (LLOD) 4 h post-dosing. The mean brain/plasma ratios for 2-Br-LSD were dose- and time-dependent and ranged from 0.27–0.75 at the 10-min point post-injection.

Effect of 2-Br-LSD on the head-twitch response in mice

The head-twitch response (HTR) is a rapid side-to-side rotational head shaking induced by psychedelic drugs in mice via 5-HT_{2A} receptor activation[47] and serves as a behavioral proxy in mice for human hallucinogen effects because non-hallucinogenic 5-HT_{2A} receptor agonists do not induce head twitches[48]. 2-Br-LSD was tested in male C57BL/6J mice over a 100-fold range of doses (0.1–10 mg/kg IP) but did not induce the HTR (Fig. 2D, $F_{5,25}$=1.91, p=0.1282). Administration of 0.1 mg/kg LSD, by contrast, produced a significant increase in HTR counts (t_9=8.35, p<0.001). Thus, 2-Br-LSD acts as a non-hallucinogenic 5-HT_{2A} agonist in mice, consistent with reports in humans.

Although 2-Br-LSD is brain penetrant (Fig. 2C), we tested whether pre-treatment with 2-Br-LSD can block the HTR induced by the psychedelic 5-HT_{2A} agonist 2,5-dimethoxy-4-iodoamphetamine (DOI), to confirm lack of HTR was not due to a low level of 5-HT_{2A} receptor occupation in the brain. As expected, 2-Br-LSD attenuated the response to DOI in a dose-dependent manner ($F_{4,26}$=17.96, p<0.0001; Fig. 2E) and produced a high level of blockade (76% attenuation at 3 mg/kg 2-Br-LSD). Additionally, we examined the time-course of the interaction between 2-Br-LSD and DOI (Fig. 2F). In mice pre-treated with 1 mg/kg 2-Br-LSD, the response to DOI was almost completely blocked during the first 10 minutes and then gradually returned to control levels after about 40–60 minutes, yielding a significant Drug × Time interaction ($F_{47,658}$=12.45, p<0.0001). These results indicate that 2-Br-LSD produces significant occupation of 5-HT_{2A} receptors in the brain for at least 30 min after IP administration, matching the pharmacokinetics of 2-Br-LSD in the mouse brain. 2-Br-LSD antagonized the effect of DOI on 5-HT_{2A} activation, providing further validation *in vitro* (Fig. 2G; K_B = 0.17 nM).

There are countervailing interactions between 5-HT_{1A} and 5-HT_{2A} receptors[49,50], and activation of 5-HT_{1A} can block the HTR induced by psychedelic drugs[51,52]. Since 2-Br-LSD acts as a potent full agonist at the 5-HT_{1A} receptor, it is possible that 2-Br-LSD's 5-HT_{1A} agonism masks the HTR[53]. We therefore tested whether 2-Br-LSD can induce the HTR in the presence of WAY-100,635. Pre-treatment with 1 mg/kg WAY-100,635 had no effect on the response to 2-Br-LSD in the HTR assay (Fig. S3D; WAY-100,635 × 2-Br-LSD interaction: $F_{1,20}$=0.12, p=0.735). These results confirm that 2-Br-LSD's 5-HT_{1A} agonism is not suppressing the HTR.

We also tested whether 2-Br-LSD's D_2 agonism could explain the lack of HTR. 2-Br-LSD did not induce the HTR after pretreatment with the selective $D_{2/3}$ antagonist *S*-(–)-raclopride (pretreatment × treatment: $F_{1,16}$=3.32, p=0.0874; Fig. S3E). In addition, although

co-administration with the $D_{2/3}$ agonist (–)-quinpirole attenuated the response to DOI ($F_{2,13}$=6.02, p=0.0141), the inhibitory effect was feeble (a ~20% reduction; Fig. S3F). Another study reported that quinpirole does not alter the HTR induced by LSD[48]. Therefore, the lack of HTR activity is not likely due to D_2 receptor activation.

2-Br-LSD has a safer cardiovascular profile compared to LSD

Chronic 5-HT_{2B} receptor activation can cause fibrotic cardiac valvulopathy[54], which necessitated the withdrawal of multiple FDA-approved drugs[55], making 5-HT_{2B} off-target activity a critical liability[56]. While LSD has robust agonist activity at 5-HT_{2B}, 2-Br-LSD failed to induce 5-HT_{2B} Gq dissociation, β-arrestin2 recruitment, or Gq-mediated calcium flux and instead demonstrated potent antagonist activity (Fig. 3A–C).

We showed above that 2-Br-LSD shows weak activity at aminergic GPCRs known to affect blood pressure, heart rate and other autonomic functions. Next, 2-Br-LSD was also tested in a Eurofins panel of 44 known off-targets (Table S5) and other transporters (Table S6), and was mostly inactive at all targets at concentrations up to 10 μM (including serotonin 5-HT_3). Exceptions were that 2-Br-LSD showed low micromolar activity at $Nav_{1.5}$ sodium channels (EC_{50} = 1.1 μM) and submicromolar activity at OCT2 (IC_{50} = 0.5 μM). Importantly, 2-Br-LSD produced a weak blockade (Fig. 3D, EC_{50} = 31.6 μM) of the hERG (K_V11.1) channel, an effect known to cause cardiac arrhythmias. Despite the detected off-target activities in the sub-micromolar range, 2-Br-LSD possesses >100-fold preference for indicated serotonin and dopamine GPCRs over these off-targets, demonstrating a safer cardiovascular toxicity profile.

2-Br-LSD produces weak 5-HT_{2A} β-arrestin recruitment and has reduced potential to induce tolerance *in vivo*

β-Arrestin recruitment is an important signaling pathway for GPCR internalization and downregulation[57], and GPCR biased agonism is an essential parameter for on-target efficacy and drug development[58]. Experiments were conducted using β-arrestin2 recruitment BRET assays to determine biased signaling differences at every 5-HT receptor except 5-HT_7 (Fig. 4A, Fig. S4A–K). We calculated the relative activity (log E_{MAX}/EC_{50}) and plotted a heat map comparing 5-HT, LSD and 2-Br-LSD activities (Fig. 4B; Table S2). At 5-HT_{1A} and 5-HT_{2C} receptors where 2-Br-LSD G protein agonism was robust, we observed no detectable β-arrestin2 recruitment agonism despite LSD and 5-HT showing similar or comparable β-arrestin2 recruitment at these receptor subtypes, indicative of G protein-bias (Fig. S4A, H). Notably, we observed very little difference in 5-HT_{2A} biased agonism for 2-Br-LSD comparing Gq to β-arrestin2 recruitment activities (Fig. S4F). Similar to Gq dissociation efficacy, 2-Br-LSD was a partial agonist for 5-HT_{2A} β-arrestin recruitment (E_{MAX} = 36.9%, Fig. 4C). To confirm the weak β-arrestin efficacy in an orthologous assay, we measured loss-of-surface of expression using a NanoBit N-terminal HiBiT-fused 5-HT_{2A} receptor. After 60 minutes of treatment, 2-Br-LSD exhibited a partial agonist effect on 5-HT_{2A} internalization (Fig. 4D), consistent with our assessment of β-arrestin2 recruitment using BRET-based assays.

Because 2-Br-LSD produces a much weaker level of β-arrestin recruitment and internalization compared to psychedelics such as DOI and LSD, studies were conducted to test whether 2-Br-LSD can induce receptor downregulation and tolerance *in vivo*. Mice received IP injections of vehicle, DOI (10 mg/kg/day), or 2-Br-LSD (3 mg/kg/day) once daily for seven consecutive days and were then challenged with DOI (1 mg/kg) 24 hours later (Fig. 4E). While repeated treatment with DOI induced a significant degree of tachyphylaxis ($p<0.001$ vs. control, Dunnett's test), no tolerance was observed on HTR after repeated treatment with 2-Br-LSD (Fig. 4F).

2-Br-LSD promotes neuronal structural plasticity

Loss of neurites, synaptic spine and contacts in cortical neurons are distinctive aspects of depression pathology[23], and neural plasticity is thought to underlie the therapeutic response to anti-depressant drugs[23–25,59,60]. To determine whether 2-Br-LSD can induce structural plasticity and increase arbor complexity, cultured primary cortical neurons were treated with 2-Br-LSD (1–100 nM) for 3 hours on day *in vitro* 3 (DIV3) and then morphological changes in dendritic arbor complexity were measured on DIV6. As an active comparator, we tested ketamine (10 μM), which induces dendritogenesis and synaptic plasticity, effects potentially underlying its antidepressant activity[59,60].

2-Br-LSD produced a dose-dependent increase in the number of dendrites crossing the Sholl radii, reaching a maximal effect at the two highest concentrations (1 and 10 μM) (Fig. 5A–B; 1-way ANOVA: $F_{6,35}=3.287$, $p=0.0114$). At those two concentrations, the effect of 2-Br-LSD was similar to the effect of ketamine (Fig. 5A–B; $p=0.0096$, control vs. ketamine, Bonferroni's test). Accordingly, 1 and 10 μM 2-Br-LSD increased the total length of the dendritic arbor compared to controls (Fig. 5A, C; 1-way ANOVA: $F_{6,35}=4.49$, $p=0.0018$).

Next, we analyzed effects of 2-Br-LSD treatment (3 h) on primary cortical neuron spine density at DIV18. An overall significant treatment effect was found 24 h after incubation onset (Fig. 5D–E, 1-way ANOVA: $F_{6.63}=22.12$, $p<0.0001$). Specifically, spine density increased after a 3-h incubation with 2-Br-LSD (1 and 10 μM) or ketamine (10 μM) compared to vehicle-treated neurons. The increase in spine density induced by 10 μM 2-Br-LSD was comparable to the effect of ketamine (Fig. 5D–E).

We also tested the effect 2-Br-LSD on the viability of cultured primary rat cortical neurons and determined it was not different from control neurons at every tested concentration (Fig. S5A; 1-way ANOVA: $F_{6,14}=0.8030$, $p=0.5838$). This indicates that dendritic complexity and dendritic spine density increase at 2-Br-LSD concentrations that do not affect neuronal viability.

2-Br-LSD promotes exploration of stressogenic environments, active coping behaviours and cortical spinogenesis *in vivo*

LSD and other psychedelics have been shown to relieve depressive symptoms in treatment-resistant MDD[10,17,61] and induce behavioral effects in rodents comparable to first-line antidepressants and rapidly acting treatments such as ketamine[5,62–64]. To test the potential therapeutic activity of 2-Br-LSD for mood disorders, we evaluated the effects of 2-Br-LSD on activity in the forced swim test (FST) and open field test (OF), which have been used

to screen antidepressant and anxiolytic drugs, respectively[65,66]. Male and female mice were treated with three doses of 2-Br-LSD (0.3, 1.0, 3.0 mg/kg) and were evaluated 24 h (OF) and 25 h (FST) later (Fig. 6A) when 2-Br-LSD has been cleared from the brain (Fig. 2C and S3A).

In the OF, neither females nor males showed a significant increase in locomotion (distance travelled) following 2-Br-LSD treatment (Fig. 6B and E; Brown-Forsythe ANOVA: $F_{3.00,29.02}$=0.1320, p=0.9403 and 1-way ANOVA: $F_{3,39}$=1.824, p=0.1587, respectively). Importantly, female mice showed increased exploration of the arena center after the 1 and 3 mg/kg treatments (Fig. 6C and S5B; 1-way ANOVA: $F_{3, 40}$=7.431, p=0.0005), with maximal effects (an increase of 88.18 ± 18.89 s) at the 1 mg/kg dose. Despite a similar trend, the increased exploration of the open field stressogenic area by 2-Br-LSD was not significant in male mice (Fig. 6F and S5B, 1-way ANOVA: $F_{3,39}$=2.005, p=0.1291). These results indicate potential anxiolytic effects of 2-Br-LSD in female mice as it increased the exploration of stressogenic environments at doses with no effect on locomotor activity.

In the FST, we observed a 35.18 ± 10.03 s decrease in immobility in females at the 1 mg/kg dose (Fig. 6D; 1-way ANOVA: $F_{3,39}$=4.438, p=0.0089). A similar effect was observed in males at all doses tested (Fig. 6G; 1-way ANOVA: $F_{3,39}$=5.739, p=0.0024). Decreases in immobility induced by the 0.3, 1 and 3 mg/kg doses in males (20.89 ± 8.249, 27.27 ± 8.226, and 31.36 ± 8.226 s, respectively) were comparable to the effect of 1 mg/kg in females.

Following FST testing, brains were collected for synaptic spine analysis ~26 h after treatment. We focused on the PFC given its central role in the response to rapidly acting antidepressants[67–70] and controlling active stress-coping behaviors[71,72]. We found a significant increase in average spine density following 2-Br-LSD treatment in both sexes compared to controls (Fig. 6H–I; females: t_{20}=2.142, p=0.0447; males: t_{21}=3.382, p=0.0028).

2-Br-LSD reverses the behavioural effects of chronic stress in mice

Chronic stress is a risk factor for many mood disorders, including MDD[73,74]. Exposure to chronic stress in rodents leads to behavioral, structural, and molecular adaptations relevant to MDD and other psychiatric disorders[75,76]. These alterations can be reversed by antidepressant treatments such as ketamine and serotonergic hallucinogens, including LSD[77,78]. To investigate whether 2-Br-LSD can reverse the dysregulated behavioral effect of chronic stress, female mice were subjected to a chronic variable stress (CVS) regime over five weeks[79], which co-terminated with two different 2-Br-LSD treatment regimes: 1 dose after the last day of stress (3 mg/kg IP; CVS 2-Br-LSD 1X 3 mg/kg group) or 4 lower doses (1 mg/kg IP; CVS 2-Br-LSD 4X 1 mg/kg group) administered every 48 hours, starting on day 28 of CVS, Fig. 6J).

In the OFT, CVS induced a 55.95 ± 19.28 s decrease in the time mice spent exploring the center of the chamber (Fig. 6L; 1-way ANOVA: $F_{3,43}$=4.649, p=0.0067) without changing total distance travelled (Fig. 6K; 1-way ANOVA: $F_{3,43}$=1.074, p=0.3702). The exploration of the arena center was increased by the repeated 2-Br-LSD treatment regime in CVS mice to levels matching the control (naïve-saline) group (4X 1mg/kg; Fig. 6L) without affecting

locomotion (Fig. 6K). The acute 2-Br-LSD treatment (1X 3 mg/kg) partially restored the effect of CVS, as this group spent time in the center of the open field intermediate between the CVS-saline and naïve-saline groups (Fig. 6L).

CVS also reduced the time spent self-grooming in the splash test (Fig. 6M; 1-way ANOVA: $F_{3,40}$=3.016, p=0.0410), an ecologically relevant measure of self-care that is sensitive to stress in mice[80]. Female mice in the CVS-1X-2-Br-LSD and CVS-4X-2-Br-LSD groups had grooming levels intermediate between naïve-saline and CVS-saline groups, indicating a partial reversal of CVS effects (Fig. 6M).

The same cohort of mice was tested 28 days after the last treatment. At this time, only the effects of CVS in the OFT were evident (Fig. S6A), while effects in the splash test appeared to have washed out (Fig. S6B). Indeed, just as during the day of treatment (Fig. 6K–L), the CVS-saline group had a persistent decrease in time exploring the center of the open field (Fig. S6A; 1-way ANOVA: $F_{3,42}$=4.337, p=0.00095) that remained reversed by the 2-Br-LSD 4X 1 mg/kg treatment regime (Fig. S6A). Overall, these data support a therapeutic effect of 2-Br-LSD against the maladaptive effects of chronic stress.

The effects of 2-Br-LSD on dendritogenesis and active coping behaviour are mediated by 5-HT$_{2A}$ activation

Given the activity of 2-Br-LSD at the 5-HT$_{2A}$ receptor, we treated primary cortical neurons with the selective 5-HT$_{2A}$ antagonist volinanserin (M100907, Vol) at 0.1–1 μM prior to the administration of 2-Br-LSD (1 μM). Calcium flux assays conducted with 5-HT-stimulated 5-HT$_2$ subtypes confirmed that Vol acts as a selective 5-HT$_{2A}$ antagonist, with greater than 240- and 5,000-fold selectivity over 5-HT$_{2C}$ and 5-HT$_{2B}$, respectively (Fig. S6C). Administered alone, Vol did not change any parameter linked to dendritic arbor complexity at any concentration assayed (Fig. 7A–C). Pre-treatment with Vol at every concentration tested blocked the effect of 2-Br-LSD on dendritic arbor complexity, as observed using Sholl intersection analysis, to levels seen in control neurons (Fig. 7A–B; 1-way ANOVA: $F_{7,32}$=12.89, p<0.0001). Accordingly, Vol also blocked the increase in total dendrite length induced by 1 μM 2-Br-LSD (Fig. 7A and C; 1-way ANOVA: $F_{7,32}$=16.70, p<0.0001).

In vitro, Vol was able to completely block the partial Gq and β-arrestin2 agonism of 2-Br-LSD at 5-HT$_{2A}$ when tested at similar concentrations (Fig. S6D,E). *In vivo*, Vol pre-treatment (0.125 mg/kg) blocked the decrease in immobility induced by 2-Br-LSD (1 mg/kg) in the FST in both females (Fig. 7D; pre-treatment × treatment interaction: $F_{1,43}$=5.32, p=0.026) and males (Fig. 7E; pre-treatment × treatment interaction: $F_{1,44}$=5.441, p=0.0243). Neither Vol nor a combination of Vol and 2-Br-LSD affected locomotion in the OF (Fig. 7F–G).

Discussion

Psychedelic drugs such as LSD and psilocybin induce intense hallucinogenic effects via 5-HT$_{2A}$ receptor activation and show promise as potential treatments for depression and anxiety. Although LSD and psilocybin appear to have considerable therapeutic efficacy and are currently being evaluated as potential medications, developing psychedelic analogs

that are therapeutic but have less hallucinogenic potential will be useful. The present investigation focused on the LSD analog 2-Br-LSD, which reportedly does not possess LSD-like activity in humans.

We found that like LSD, 2-Br-LSD acts as an agonist at a wide range of aminergic GPCRs. LSD is nearly a full agonist at the 5-HT_{2A} and 5-HT_{2B} subtypes, whereas 2-Br-LSD acts as a partial agonist at 5-HT_{2A} and a potent antagonist at 5-HT_{2B}. In addition to activating the 5-HT_{2A} receptor, LSD interacts with many other aminergic GPCRs, potentially resulting in side-effects, but we found that 2-Br-LSD has less off-target activity compared to LSD and possesses weak micromolar activity at other ion channels, including hERG channels. Taken together, 2-Br-LSD possesses a favorable profile as a drug candidate, with less potential for side-effects compared to other serotonergic drugs, such as fenfluramine and methysergide.

Importantly, 2-Br-LSD did not induce head twitches in mice despite acting as a potent 5-HT_{2A} partial agonist. The mouse HTR assay shows a high level of sensitivity to 5-HT_{2A} agonists[81], and hundreds of compounds have been tested in the assay. Lisuride, an LSD analog that acts as a partial 5-HT_{2A} agonist, fails to induce hallucinogenic effects in humans and is inactive in the HTR paradigm[48,82]. One unanswered question is why lisuride and 2-Br-LSD lack hallucinogenic potential and fail to induce the HTR. One possible explanation is that the level of 5-HT_{2A} activation produced by 2-Br-LSD and lisuride may not be sufficient to induce head twitches. Our study determined that 2-Br-LSD is a weaker 5-HT_{2A} partial agonist compared to LSD and other psychedelic drugs[83] and can partially antagonize 5-HT_{2A}. In previous studies, the peak HTR rate correlated with 5-HT_{2A} agonist efficacy[84], which suggests that weaker 5-HT_{2A} partial agonism may explain why 2-Br-LSD does not induce the HTR. These HTR results support 2-Br-LSD's lack of hallucinogenic potential in humans and provide evidence that 2-Br-LSD can block subjective responses to LSD in some human trials[34,85] via occupation of 5-HT_{2A}.

The HTR data with 2-Br-LSD are consistent with its reported effects in humans and support its classification as a non-hallucinogenic 5-HT_{2A} agonist. Five cluster headache patients who received 30 μg/kg 2-Br-LSD orally on three occasions experienced only minor side effects, such as feeling "slightly tipsy"[31]. Higher oral doses, ranging from 64–256 μg/kg, induced mild subjective responses, including restlessness, anxiety, drowsiness, impaired concentration, and euphoria[30,86]. Intravenous infusion of 18–22 μg/kg 2-Br-LSD produced more intense effects, such as depersonalization, derealization, and mild confusion[87]. However, none of the subjects who received 2-Br-LSD orally or intravenously experienced visual hallucinations or profound cognitive alterations similar to those induced by LSD. Although 2-Br-LSD may produce some psychoactive effects in humans after administration of very high dosages, it clearly does not act as a psychedelic like LSD.

Repeated treatment with psychedelic drugs downregulates 5-HT_{2A} receptor signaling and induces a rapid behavioral tolerance in rodents[1,49,88–91] and humans[92,93]. The tachyphylaxis induced by LSD and psilocybin limits how frequently those drugs can be administered to patients. Notably, in our study, mice treated with 2-Br-LSD for seven consecutive days did not show evidence of tachyphylaxis. The absence of tolerance with 2-Br-LSD may be a consequence of its weak recruitment of 5-HT_{2A} β-arrestin2, which have been shown to

bind 5-HT_{2A} *in vitro* and are co-localized in pyramidal neurons[94]. It was reported recently that β-arrestin2 knockout mice show tolerance to the HTR-inducing effects of LSD after repeated treatment[95] indicating β-arrestin2 recruitment may not play a role in the tolerance to psychedelics. However, the relevance of those findings to wild-type mice is unclear because there would likely be considerable re-organization or compensation of GPCR signaling after global deletion of the β-arrestin2 gene. The same line of knockout mice has been used to investigate the role β-arrestin2 recruitment plays in respiratory depression induced by μ-opioid receptor agonists[96], but the results have been called into question by subsequent studies[97,98]. In summary, compared to psychedelic drugs, 2-Br-LSD produces less recruitment of β-arrestin2 via 5-HT_{2A} and fails to produce tolerance *in vivo*.

Our results indicate that 2-Br-LSD has effects comparable to those of classical psychedelic drugs, which have been shown to produce lasting anti-depressant-like effects. For example, psilocybin treatment increased dendritogenesis and spinogenesis in rodents[5] and produced rapid and lasting anti-depressant effects in human clinical trials[16,17,61,99]. LSD has also been shown to produce antidepressant effects in humans[44], enhance neuroplasticity in rat neuronal cultures, and promote hippocampal neuronal proliferation and spinogenesis[5,24,100,101]. Finally, studies with the psychedelic drug 5-methoxy-*N,N*-dimethyltryptamine showed an increase in dendritic arbour complexity and spine density in cultured rat cortical neurons[101,102]. These classic psychedelics all share 5-HT_{2A} receptor agonism, considered to be a fundamental component in their anti-depressant activity. We confirmed the likely 5-HT_{2A} dependency of their anti-depressant-like effects[6] by testing whether the 5-HT_{2A} antagonist volinanserin can block 2-Br-LSD's activities. These results suggest that 2-Br-LSD has the potential to be an effective treatment for MDD, possibly through its effects on neuroplasticity.

The loss of dendrite arbor complexity, retraction of neurites and dendritic spines, and reduced synaptic density represent negative structural changes observed in the PFC of patients suffering from depression and anxiety[103]. Compounds modifying synaptic plasticity are considered promising therapies for those disorders. Indeed, a central hypothesis for the mechanism of action for the therapeutic antidepressant effects of psychedelics involves the rapid induction of structural and functional neural plasticity and the reversal of neuronal atrophy[18,23–25]. While a direct link between neuroplasticity and the behavioral effects of psychedelic drugs has yet to be shown, the hypothesis of neuronal atrophy reversal may explain why psychedelics produce effects persisting after treatment has ceased. The NMDA receptor antagonist ketamine, a dissociative anesthetic drug with hallucinogenic effects, produces well-described anti-depressant effects after a few treatments coupled with changes in arbor complexity and spine density, effects thought to be linked[60]. While the primary receptor targets of dissociative anesthetics and psychedelic drugs are different, they both show similar downstream effects *in vivo* and *in vitro*, suggesting that their effects on neuroplasticity and neuronal atrophy may serve as a common pathway for the treatment of MDD and anxiety disorders. We show that 2-Br-LSD induces spinogenesis *in vivo* and *in vitro* in two rodent species and produces effects on chronic stress, which together suggest that 2-Br-LSD may have therapeutic potential for the treatment of depression, anxiety, and potentially other psychiatric disorders. Finally, the lack of 2-Br-LSD tolerance and 5-HT_{2B} agonist activity may permit frequent dosing for mood disorders and other indications.

Limitations of the study

Several limitations are noted for this study. First, *in vitro* GPCR assays may not reflect efficacy *in vivo* due to the measurement of specific G protein and β-arrestin subtypes, which may be cell-type specific. Moreover, not all GPCR effectors and signaling pathways were studied. Assessment of hallucinogenic potential using HTR testing has limitations because it may not model the human psychedelic state. Although HTR data support the classification of 2-Br-LSD as a non-hallucinogenic 5-HT_{2A} agonist, its activity ultimately must be defined based on human data. Although it cannot be excluded that the lack of hallucinogenic effects is a consequence of the dose range tested, pretreatment with 2-Br-LSD attenuated the response to LSD in some studies[34,85] further indicating 2-Br-LSD is capable of engaging 5-HT_{2A} receptors in brain. However, additional clinical studies are required to fully characterize the effects of 2-Br-LSD in humans and understand its subjective phenomenology. Finally, FST has been widely used for testing novel antidepressant drugs, but its utility has been questioned due to a lack of face and predictive validity[104–106]. Therefore, we used additional tests to determine whether 2-Br-LSD produces antidepressant-like effects, including the chronic stress model which has greater construct validity for the pathological alterations leading to depression[107]. Despite obtaining concordant results in both paradigms, the potential antidepressant effects of 2-Br-LSD must be confirmed in additional preclinical behavioral models of depression (e.g., chronic social defeat) and using additional physiological outcomes relevant to depression (e.g., inflammatory markers, HPA axis activation).

STAR Methods

RESOURCE AVAILABILITY

Lead Contact—Further information and requests for resources and reagents should be directed to and will be fulfilled by the lead contact, John D. McCorvy (jmccorvy@mcw.edu)

Materials Availability—All plasmids and cells generated from this study could be obtained directly from lead contact with a completed Materials Transfer Agreement if there is potential for commercial application.

Data and code availability

- All data generated in this study are included in this article and the supplemental information. All data reported in this paper will be shared by the lead contact upon request.
- Custom code can be obtained from github as indicated in Key Resource Table.
- Any additional information required to reanalyze the data reported in this paper is available from the lead contact upon request.

EXPERIMENTAL MODEL AND SUBJECT DETAILS

In vitro GPCR signaling studies utilized human embryonic kidney (HEK) derived-cell lines, HEKT (ATCC) and Flp-In T-Rex 293 (Invitrogen). Cell lines were cultured in a humidified

incubator at 37°C at 5% CO_2 in high-glucose DMEM (VWR) supplemented with 10% FBS (Life Technologies), and authenticated and tested to be mycoplasma-free. Sex of HEK-derived cell lines are female. Male and female CD-1 mice (Charles River Laboratories Inc, Wilmington, MA, USA) were used to assess the pharmacokinetics of 2-Br-LSD. The study was reviewed and approved by Animal Care Committee of Nucro-Technics Inc (Scarborough, ON, Canada) and was performed in accordance with their standard operating procedures. Male C57BL/6J mice (6–8 weeks old) from Jackson Labs (Bar Harbor, ME, USA) were used for the head-twitch response (HTR) experiments. The mice were housed on a reversed light-dark cycle (lights on at 1900 h, off at 0700 h,) in an AALAC-approved vivarium at the University of California San Diego (UCSD). Mice were housed up to four per cage in a climate-controlled room and with food and water provided *ad libitum* except during behavioral testing. Testing was performed between 1000 and 1800 h (during the dark phase of the light-dark cycle). The studies were conducted in accordance with National Institutes Health (NIH) guidelines and were approved by the UCSD Institutional Animal Care and Use Committee. For primary neuronal cultures, gestating Sprague-Dawley rats (Charles River Laboratories) were used at gestation day (GD) 18. For *in vivo* depression-relevant behavioral models (forced swim and open field tests in non-stressed mice), adult male and female C57BL/6 mice (7–8 weeks old) were obtained from Jackson Laboratories. For chronic stress experiments, 8 weeks old female mice were obtained from Charles River Laboratories (as indicated below). Mice were housed in Carleton University's vivarium for at least 2 weeks of acclimatization before being experimental procedures started. Mice were housed in groups of four and kept in a 12:12 light/dark cycle with water and food pellets *ab libitum*, in temperature- and humidity-controlled rooms (21°C, ~55% humidity), except for chronic stress experiments where housing conditions varied as described below. All experimental procedures involving animals were approved by Carleton University's Animal Care Committee, pursuant of the Canadian Council of Animal Care guidelines.

METHOD DETAILS

Compounds—(6a*R*,9*R*)-2-bromolysergic acid diethylamide (2:1) (+)-tartrate (2-Br-LSD; BETR-001) was obtained from BetterLife Pharma (Vancouver, BC, Canada). For *in vivo* studies, 2-Br-LSD was dissolved in 0.9% saline. For *in vitro* pharmacological studies, a 10 mM stock solution of 2-Br-LSD was prepared in DMSO and stored at −80°C. For cell culture experiments, 2-Br-LSD was dissolved in molecular grade water (2 M concentration) and then diluted with Neurobasal medium (Thermo Fisher Scientific). For *in vivo* studies, (+)-lysergic acid diethylamide (2:1) (+)-tartrate (LSD) was obtained from the National Institute of Drug Abuse (NIDA) Drug Supply Program (Bethesda, MD, USA) and dissolved in 0.9% saline. For *in vitro* studies, LSD tartrate was obtained from Sigma-Aldrich (St. Louis, MO, USA). (±)-2,5-Dimethoxy-4-iodoamphetamine hydrochloride (DOI) was obtained from Cayman Chemical Co. (Ann Arbor, MI, USA) and dissolved in 0.9% saline. *N*-[2-[4-(2-Methoxyphenyl)-1-piperazinyl]ethyl]-*N*-(2-pyridinyl)cyclohexanecarboxamide maleate (WAY-100,635) was obtained from the NIMH Chemical Synthesis and Drug Supply Program (Rockville, MD, USA) and dissolved in sterile water. *S*-(–)-Raclopride (+)-tartrate and (–)-quinpirole hydrochloride were obtained from Sigma-Aldrich and dissolved in 0.9% saline. Ketamine hydrochloride (Bimeda Canada, Cambridge, ON, Canada) was diluted with 0.9% saline for *in vivo* experiments or diluted

with Neurobasal medium for *in vitro* experiments. For *in vitro* experiments, the 5-HT_{2A} selective antagonist volinanserin (M100,907; Cayman Chemical Co.) was dissolved in 10% DMSO and diluted with Neurobasal medium; the vehicle control consisted of Neurobasal medium containing 0.1% DMSO. For *in vivo* assays, volinanserin was dissolved in 1 M HCl, the pH was adjusted to 7.2 using 1 M NaOH, and then 0.9 % saline was added to bring the solution up to full volume; the vehicle control consisted of 1 M HCl adjusted to pH 7.2 and brought up to full volume with 0.9% saline. All *in vivo* drug treatments were administered intraperitoneally (IP) with an injection volume of 5 mL/kg or 10 mL/kg body weight.

GPCR G protein-dissociation and β-arrestin2 recruitment BRET assays—All BRET assays were conducted using $BRET^2$ in HEK293T cells (ATCC CRL-11268; mycoplasma-free), which were subcultured in high-glucose DMEM (VWR) supplemented with 10% FBS (Life Technologies). Constructs in G protein-dissociation BRET assays were derived from the codon-optimized Tango pcDNA3.1 library[108] (Addgene) with V2tail/TEV/tTA encoding regions deleted to yield “de-Tango” constructs. All Gα-Rluc8 and GFP^2-γ constructs were derived from TRUPATH library[38] (Addgene), and pcDNA3.1-Gβ and human-β-Arrestin2 constructs were purchased from cDNA Resource Center; www.cDNA.org. N-terminal GFP^2-fused human β-Arrestin2 constructs were created using templates from addgene and cdna.org, and subcloned into pcDNA3.1. 5-HT receptor constructs used in β-Arrestin2 recruitment BRET assays were also derived from the Tango library with V2tail/TEV/tTA encoding regions replaced with *Renilla* luciferase (Rluc8) using Gibson Assembly. Constructs from human GRK2 were synthesized from IDT and subcloned into pcDNA3.1. Approximately 48 hours before assays, cells were transfected using a reverse transfection method and plated in 1% dialyzed FBS (dFBS) at an approximate density of 15,000 cells per well into poly-L-lysine-coated 384-well white assay plates (Grenier Bio-One). For G protein-dissociation assays, cells were transfected in an indicated ratio of receptor: Gα-Rluc8: Beta: GFP^2-γ constructs (see Supplement for ratios). For β-Arrestin2 recruitment assays, cells were transfected at a ratio of 5-HTR-Rluc8: GFP^2-fused human β-Arrestin2 (see Table S1). All transfections were prepared in Opti-MEM (Invitrogen) and used a 3:1 ratio of TransIT-2020 (Mirus) uL:ug total DNA. On the day of the assay, plates were decanted and 20 uL of drug buffer per well (1× HBSS, 20 mM HEPES, pH 7.4) was added using a Multidrop (ThermoFisher Scientific), and plates were allowed to equilibrate at 37°C in a humidified incubator before receiving drug stimulation. Drug dilutions of all compounds were performed in McCorvy buffer (1× HBSS, 20 mM HEPES, pH 7.4, supplemented with 0.3% BSA fatty acid free (GoldBio), and 0.03% ascorbic acid). Drugs were dispensed using a $FLIPR^{TETRA}$ (Molecular Devices). Next, plates were incubated at 37°C in a humidified incubator for 60 minutes or specified time point (see Supplement). Before reading, addition of coelenterazine 400a (5 uM final concentration; Nanolight Technology) was performed by the $FLIPR^{TETRA}$.

Calcium Flux Assays—Stable-expressing 5-$HT_{2A/2B/2C}$ receptor Flp-In 293 T-Rex Tetracycline inducible cell lines (Invitrogen, mycoplasma-free) were used for Gq-mediated calcium flux assays. Constructs used for these assays were derived from the codon-optimized Tango pcDNA3.1 library[108] (Addgene) with V2tail/TEV/tTA encoding regions

deleted to yield “de-Tango” constructs, and then subcloned into pcDNA5/FRT/TO using Gibson Assembly. Cell lines were maintained in high-glucose DMEM (VWR) containing 10% FBS (Life Technologies), 10 μg/mL Blasticidin (GoldBio), and 100 μg/mL Hygromycin B (GoldBio). Approximately 24 hours before the assay, receptor expression was induced with tetracycline (2 ug/mL) and seeded into 384-well poly-L-lysine-coated black plates at a density of approximately 7,500 cells/well in DMEM containing 1% dialyzed FBS. On the day of the assay, plates were decanted and cells were incubated with Fluo-4 Direct dye (Invitrogen, 20 μl/well) for 1 h at 37°C, which was reconstituted in drug buffer (1× HBSS, 20 mM HEPES, pH 7.4) containing 2.5 mM probenecid. After dye load, cells were allowed to equilibrate to room temperature for 15 minutes, and then placed in a FLIPR^{TETRA} fluorescence imaging plate reader (Molecular Devices). Drug dilutions were prepared at 5× final concentration in McCorvy buffer (20 mM HEPES-buffered HBSS, pH 7.4 supplemented with 0.3% BSA fatty-acid free and 0.03% ascorbic acid). Drug dilutions were aliquoted into 384-well plastic plates and placed in the FLIPR^{TETRA} for drug stimulation. Fluorescence for the FLIPR^{TETRA} were programmed to read baseline fluorescence for 10 s (1 read/s), and afterward 5 μl of drug per well was added and read for a total of 5 min (1 read/s).

cAMP Accumulation and Inhibition GloSensor™ Assays—HEK293T cells (ATCC CRL-11268; mycoplasma-free) were co-transfected in 1:1 ratio with “de-Tango” plasmids described above and GloSensor-22F plasmid (Promega). Cells were transfected in 10% dFBS, and next day cells were plated into poly-L-lysine-coated 384-well white assay plates (Grenier Bio-One) at a density of approximately 15,000 cells per well. After approximately 48 hours post-transfection, plates were decanted and 20 uL per well of drug buffer (1× HBSS, 20 mM HEPES, pH 7.4) containing 4 mM D-luciferin (sodium salt; GoldBio) was added using a Multidrop (ThermoFisher Scientific). Cells were allowed to equilibrate for approximately 15 minutes at room temperature, and then challenged with serial dilution of drugs (diluted in McCorvy buffer, see above), dispensed by a FLIPR^{TETRA}. For Gi/o-coupled receptors, cells were incubated with drugs for exactly 15 minutes at room temperature and then challenged with 0.2 μM isoproterenol (final concentration) to stimulate endogenous cAMP via endogenously expressed β-adrenergic receptors in HEK cells. Plates were then read for luminescence (LCPS) 15 minutes later, for a total of 30-minute drug incubation on a Microbeta Trilux (PerkinElmer). For Gs-coupled receptors, cells were incubated for exactly 30 minutes at room temperature and also read for luminescence (LCPS).

Surface Expression/Internalization Assays—Surface expression was measured using a HiBiT-tagged 5-HT$_{2A}$ receptor and the Nano-Glo HiBit Extracellular Detection System (Promega). N-terminal HiBiT-tagged human 5-HT$_{2A}$ was cloned into pcDNA3.1 using Gibson Assembly. HEK293T cells (ATCC CRL-11268; mycoplasma-free) were transfected into 10-cm tissue culture dishes in a 1:15 ratio of HiBiT-tagged human 5-HT$_{2A}$: human β-Arrestin2 (cDNA Resource Center; www.cDNA.org). Cells were transfected in DMEM 10% dFBS and the next day, cells were plated into either poly-L-lysine-coated 384 or 96-well white assay plates (Grenier Bio-One). On the day of the assay, plates were decanted and HEPES-buffered DMEM without phenol-red (Invitrogen) was added per well. Plates were

allowed to equilibrate at 37°C in a humidified incubator before receiving drug stimulation. Compounds (including 5-HT as control) were serially diluted in McCorvy buffer (20 mM HEPES-buffered HBSS, pH 7.4 supplemented with 0.3% BSA fatty-acid free and 0.03% ascorbic acid), and dilutions were added to plates either in triplicate (384) or duplicate (96). Plates were allowed to incubate at 37°C for 1 hour in a humidified incubator or a specified time point. Approximately 15 minutes before reading, LgBit and coelenterazine h (5 uM final concentration) were added to each well. Plates were sealed to prevent evaporation and read on either a PheraStar FSX (BMB Lab Tech) or Mithras LB940 (Berthold Technologies) at 485 nm at 37°C for time-capture quantification of internalization or loss of surface expression.

Analysis of 2-Br-LSD pharmacokinetics

Sample collection: Three groups of mice (n = 24 males and 24 females per group) were treated with 2-Br-LSD (0.75, 2.25, or 6.75 mg/kg); in each group, three mice/sex were sacrificed to collect plasma and brain samples pre-dose and 0.17, 0.5, 1, 2, 4, 8, and 24 h post-dose. Blood samples (~0.6 mL) were collected via cardiac puncture in tubes containing K_2EDTA anticoagulant and kept on ice prior to centrifugation (3000 rpm × 15 min) to separate the plasma. Immediately after collection of blood samples, the whole brain was collected from each mouse. Plasma and brain samples were stored at −80°C prior to analysis.

Sample extraction: To extract the plasma samples, 200 μL of acetonitrile containing 10 ng/mL LSD-d_3 (Sigma-Aldrich) was added to 50 μL of plasma. The mixture was vortexed vigorously, centrifuged (13,000 rpm) for 2 min at 4°C, and then 50 μL of supernatant was combined with 200 μL methanol/water (1:1, v/v) in a pre-labeled autosampler vial. Brains were weighed and homogenized for ~1 min in cold acetonitrile at a ratio of 1:1.5 (w/v) brain tissue to extraction solvent. The brain samples were then centrifuged at 13,000 rpm for 2 min at 4°C and the supernatant was collected in a pre-labeled autosampler vial. Seven calibration standards and four quality control samples (prepared by spiking blank K_2EDTA plasma with acetonitrile containing 100 μg/mL 2-Br-LSD) were extracted at the same time as the analytical samples.

Equipment: Samples were analyzed using an Agilent 6400 Series Triple Quadruple MS (Santa Clara, CA, USA) coupled to an Agilent 1200 Liquid Chromatography system consisting of a degasser, a binary pump and an autosampler.

LC-MS/MS method: Isocratic elution was performed on an ACE Excel 5 SuperC18TM (150 mm × 4.6 mm inner diameter, 5 μm particle size) column (Advanced Chromatography Technologies Ltd, Aberdeen, UK) at 25 °C, with a run time of 6.5 min (adjusted ±10% depending on peak elution time). The mobile phase consisted of methanol-water (8:2, v/v) plus 0.1% NH_4OH at a flow rate of 0.8 mL/min. The injection volume was 10 μL/sample. For the MS/MS analysis, electrospray ionization was used in positive ion mode (gas temperature 350°C, gas flow 13 L/min; nebulizer 60 psi, capillary voltage 4 kV).

Head-twitch response studies—Head twitches were recorded using a head-mounted neodymium magnet and a magnetometer detection coil, as described previously[82]. The mice were allowed to recover from the magnet implantation surgeries for at least 1 week prior to behavioral testing. HTR experiments were conducted in a well-lit room and the mice were allowed to habituate to the room for at least 1 h prior to testing. Immediately after drug treatment, mice were placed in a 12-cm diameter glass cylinder surrounded by a magnetometer coil and behavior was recorded continuously. Coil voltage was low-pass filtered (1 kHz), amplified, and digitized (20-kHz sampling rate) using a Powerlab 8/35 with LabChart ver. 8.1.19 (ADInstruments, Colorado Springs, CO, USA).

In the first HTR experiment, 6 groups of mice (n = 5–6/group, 36 total) were treated with vehicle, 2-Br-LSD (0.1, 0.3, 1, 3, or 10 mg/kg), or LSD (0.1 mg/kg), and HTR activity was assessed for 60 min. In the second experiment, 5 groups of mice (n = 6–7/group, 31 total) were treated with vehicle or 2-Br-LSD (0.1, 0.3, 1, or 3 mg/kg); 10 min later, all of the mice were injected with DOI (1 mg/kg) and then HTR activity was assessed for 30 min. In the third experiment, 2 groups of mice (n = 8/group, 16 total) were treated with vehicle or 2-Br-LSD (1 mg/kg); 10 min later, all of the mice were injected with DOI (1 mg/kg) and then HTR activity was assessed for 240 minutes. In the fourth experiment, 4 groups of mice (n = 6/group, 24 total) were treated with vehicle or WAY-100,635 (1 mg/kg); 20 min later, the mice were treated with vehicle or 2-Br-LSD (3 mg/kg) and then HTR activity was assessed for 30 min. In the fifth experiment, 4 groups of mice (n = 5/group, 20 total) were treated with vehicle or S-(−)-raclopride (1 mg/kg); 20 min later, the mice were treated with vehicle or 2-Br-LSD (3 mg/kg) and then HTR activity was assessed for 30 min. In the sixth experiment, 3 groups of mice (n = 5–6/group, 16 total) were treated with vehicle or (−)-quinpirole (0.025 or 0.25 mg/kg); 30 min later, all of the mice were injected with DOI (1 mg/kg) and then HTR activity was assessed for 30 min. In the seventh experiment, 3 groups of mice (n = 7/group, 21 total) received 7 daily injections of vehicle, DOI (10 mg/kg/day), or 2-Br-LSD (3 mg/kg day); 24 h after the final injection, all of the mice were injected with DOI (1 mg/kg) and then HTR activity was assessed for 30 min.

Cortical neuronal culture—For primary neuronal cultures, gestating Sprague-Dawley rats were obtained from Charles River Laboratories, at gestation day (GD) 18. Briefly, embryos were removed from the uterus of a euthanized dam and placed in dissecting solution (Hank’s balanced salt solution, 1 M HEPES, 1 % penicillin-streptomycin and glucose; Fisher Scientific). Cortices were immediately dissected from each pup and placed in chilled neurobasal medium (see below). Cortical tissue was then dissociated using TrypLE Express (Gibco) and mechanical disaggregation. Single cells were then plated at a density of 50 000 cells per well on poly-D-lysine coated glass coverslips. The initial plating medium consisted of 1% penicillin-streptomycin, 0.5 mM Glutamax (Thermo Fisher Scientific), and B-27 Plus supplement (Thermo Fisher Scientific) in Neurobasal Plus (Thermo Fisher Scientific). Plating medium was exchanged at 24 h for maintenance media with the same components, except Glutamax. Following this initial change, 50% media changes occurred at 3-day intervals. An additional 10% of the maintenance media was added during each change to account for evaporation,. Cultures were maintained at 37°C under

5% CO_2. Overall, each treatment condition was replicated in 6 independent wells, from 2 different cultures (3 wells per culture).

To assess dendritogenesis: cortical neurons maintained until day *in vitro* 3 (DIV3) and then treated with 2-Br-LSD (1 nM, 10 nM, 100 nM, 1 μM, 10 μM), ketamine (10 μM), or vehicle. Each treatment lasted 3 h, followed by a full media change. Plates were then maintained for an additional 69 h before fixation. Spinogenesis was assessed in a follow-up experiment; cortical neurons were maintained until DIV18 and treated with 2-Br-LSD (1nM, 10nM, 100nM, 1μM, 10μM), 10uM ketamine or vehicle (3 wells/plate).

Neurons were fixed by replacing 80% of the medium with 4% paraformaldehyde for 20 min, then 0.2% Triton-X was added for another 20 min. Dendritogenesis plates were then blocked with 3% BSA, and a primary antibody against the microtubule-associated protein 2 (MAP2) was added (chicken polyclonal anti-MAP2 antibody; 1:5000, EnCor Biotechnology Inc., cat. # CPCA-MAP2) overnight, followed by an incubation with a secondary antibody for 1 h (goat anti-chicken IgY (H+L) secondary antibody, Alexa Fluor 594; 1:2000; Invitrogen). Spinogenesis plates were also blocked with 3% bovine serum albumin, then fixed and stained on DIV 19, following the dendritogenesis protocol, with the addition of F-actin staining with phalloidin (Alexa Fluor 488 Phalloidin, Thermo Fisher). Culture coverslips were mounted using Vectashield mounting media containing DAPI nuclear staining (Vector Laboratories).

In a different set of cultures, to test the effects of the 5-HT_{2A} antagonist volinanserin on 2-Br-LSD action, cultured cells were treated as follows: vehicle, volinanserin alone (100 nM, 500 nM, or 1 μM), 2-Br-LSD alone (1 μM), or volinanserin (100 nM, 500 nM, or 1 μM) plus 2-Br-LSD (1 μM) (3 wells/plate). Volinanserin or vehicle was applied for 1 h before being washed out with a full media change, which was immediately followed by 2-Br-LSD treatment for 3 h.

Cell viability assays: To test the effect of 2-Br-LSD on cell viability, primary cortical neurons were cultured as for the dendritogenesis experiment above. On DIV6 (69 h after treatment), viability was assessed using the Neurite Outgrowth Staining Kit (Thermo Fisher). This assay consists of two stains, one for cell membranes in living and dead cells and one that only fluoresces when metabolized by a live cell.

Imaging dendritogenesis and spinogenesis: Neurons from the dendritogenesis and spinogenesis experiments were imaged with a Zeiss confocal laser scanning microscope (LSM 700), using an oil immersion 63× objective at 2× zoom and 1024 × 1024 pixel resolution. The spectral detectors were adjusted to capture emission from a helium/neon laser at wavelengths of 488–594 nm for Alexa Flour staining of MAP2 and F-Actin, and the pinhole diameter was maintained at 1 Airy unit. The image acquisition was set at a range of 8 bits.

In vivo models of depression

Open field test (OFT): The open field test (OFT) consisted of mice being placed in 1:1.4 ratio rectangular transparent arenas (45 cm length, 30 cm width) in a well-lit room, with

black cardboard barriers preventing mice from seeing conspecifics during testing. Mice were allowed to explore the arena for 10 minutes.

Forced-swim test (FST): For FST, mice were placed in a four-liter cylindrical glass container filled with 3 L of water at 25±1°C and filmed using a digital camera for 6 minutes.

To assess the *in vivo* effects of 2-Br-LSD, adult male and female C57BL/6J mice (Jackson laboratories) were treated with a single injection of 2-Br-LSD (0.3, 1 and 3 mg/kg) or vehicle. Mice were tested in the open field 24 h after drug treatment, followed by assessment in the FST 1 h later (n=12/group/sex). To investigate the role of the 5-HT_{2A} receptor in the effects of 2-Br-LSD, a separate cohort of male and female mice were treated with vehicle or the 5-HT_{2A} selective antagonist VOL (0.125 mg/kg) 15 min before treatment with vehicle or 2-Br-LSD (1 mg/kg). Twenty-four hours later, the mice were tested in the OFT, followed 1 h later by the FST.

Immediately following behavioural testing, mice were sacrificed, and the brains were removed and bisected; the right hemisphere was flash frozen, while the left hemisphere was processed using the FD Rapid Golgi Stain Kit protocol (FD NeuroTechnologies, Inc).

Golgi staining: To test the effects of 2-Br-LSD on spine density *in vivo*, we prepared the left hemisphere of brains from the stress-naïve experimental animals and subjected them to Golgi-Cox staining (FD Rapid GolgiStain Kit, FD NeuroTechnologies, INC). Briefly, brains were placed into the impregnation solution A/B (5% potassium dichromate, 5% mercuric chloride and 5% solution of potassium chromate), in the dark at ~25°C for 14 days. Brains were then placed in solution C (5% potassium dichromate, 5% mercuric chloride), and stored for a further 7 days. Following this, brains were removed from solution and stored at −80°C. Then 150 μm coronal cryosections were collected using a cryostat (Epredia Microm HM525 NX, Fisher Scientific), focusing on the prefrontal cortex. After cryosection, final treatment consisted of rinsing with distilled water twice for 10 min, 50 % ethanol dehydration, ammonia incubation for 15min, 5% sodium thiosulfate incubation in the dark, gradient ethanol dehydration (50–100%), xylene clearing and mounting. Imaging was done using an Olympus BX51 brightfield microscope with a 100x objective, running the Neurolucida imaging analysis software suite (Neurolucida 360/Explorer).

Chronic variable stress (CVS): CVS consisted of mild stressors administered twice daily for 33 days to single-housed female mice. Stressors' order of application was pseudo-randomized and consisted of cage tilt (at a 45° angle for 4–8 h), restraint (10 min), wet bedding (overnight), forced swim (10 min), odour exposure (animals exposed to a cotton swab embedded with lemon or cinnamon extract for 4–8 h) and/or disrupted light cycle (lights left on overnight). Control mice were also singled-housed and left undisturbed, except for a weekly handling and weighing session. Control and stressed mice were housed in separate rooms. On day 28 of stress, mice were randomly grouped into 4 groups and subjected to the following treatments (n=12/group): naïve-vehicle, CVS-vehicle, CVS-1X 2-Br-LSD (3 mg/kg) or CVS-4X 2-Br-LSD (1 mg/kg). Mice were injected every 48 h until day 34 (24 h after the last stressor for the CVS groups), for a total of 4 injections. The CVS-1X 2-BrLSD group received three vehicle injections and one injection of 2-Br-LSD,

while the group CVS-4X 2-BrLSD received 4 doses of 2-Br-LSD. Behavioral testing began 2 h following the final injection and consisted of the splash test (ST), followed by OFT (performed 2 h after the ST, as described above). A similar series of tests were performed 4 weeks later to determine whether the effect of 2-Br-LSD is long lasting.

For the ST, mice were placed in a new cage similar to their home cage for 10 min, 500 μL of a 30% sucrose solution was applied to their back, and their behavior was video recorded for 10 min.

QUANTIFICATION AND STATISTICAL ANALYSIS

GPCR G protein-dissociation and β-arrestin2 recruitment BRET assays—Plates were read at 400 nm Rluc8 and 510 nm GFP^2 emission filters for 0.8 seconds per well using a PheraStarFSX (BMB Lab Tech). The BRET ratios of 510/400 luminescence were calculated per well and were plotted as a function of drug concentration using Graphpad Prism 5 or 9 (Graphpad Software Inc., San Diego, CA). Data were analyzed using nonlinear regression “log(agonist) vs. response” to yield E_{MAX} and EC_{50} parameter estimates. Relative activities (log (E_{MAX}/EC_{50}) were calculated based on normalized data. Antagonist affinities (K_B) were calculated according to the method by Cheng utilizing EC_{50} and competing agonist concentration for each individual receptor subtype[109]. Data were normalized to % positive control stimulation and a positive control concentration-response curve was present on every plate.

Calcium Flux Assays—Fluorescence in each well was normalized to the average of the first 10 reads for baseline fluorescence, and then either maximum-fold peak increase over basal or area under the curve (AUC) was calculated. Both peak and AUC was plotted as a function of drug concentration, and data were normalized to percent 5-HT stimulation. Data were plotted and non-linear regression was performed using “log(agonist) vs. response” in Graphpad Prism 9 to yield E_{MAX} and EC_{50} parameter estimates. Data were normalized to % 5-HT response, and a positive control concentration-response curve was present on every plate.

cAMP Accumulation and Inhibition GloSensor™ Assays—LCPS was plotted as a function of drug concentration and non-linear regression was performed using “log(agonist) vs. response” in Graphpad Prism 9 to yield E_{MAX} and EC_{50} parameter estimates. Data were normalized to % 5-HT response, and a positive control concentration-response curve was present on every plate.

Surface Expression/Internalization Assays—Luminescence was plotted as a function of drug concentration using Graphpad Prism 5 or 9 (Graphpad Software Inc., San Diego, CA). Data were analyzed using nonlinear regression “log(agonist) vs. response” to yield E_{MAX} and EC_{50} parameter estimates and normalized to % 5-HT loss of surface expression, and a positive control concentration-response curve was present on every plate.

2-Br-LSD pharmacokinetics—2-Br-LSD was quantified by selected reaction monitoring of the following mass transitions (2-Br-LSD m/z 403.3 → 302, LSD-d_3 (internal standard) m/z 327.2 → 226.1. The quantification of 2-Br-LSD concentration in samples was achieved

by using appropriate calibration standards. The calibration curve was fitted linearly using a weighting factor ($1/x^2$). The pharmacokinetic parameters were determined by the non-compartmental analysis using the validated Phoenix®WinNonlin® version 8.2 software (Certara Inc).

Head-twitch response studies—Head twitches were identified in the recordings using artificial intelligence[110]. HTR counts were analyzed using one-way or two-way ANOVAs; Dunnett's test or Tukey's test was used for *post hoc* comparisons. Significance was demonstrated by surpassing an α level of 0.05. Median effective doses (ID_{50} values) and 95% confidence intervals for dose-response experiments were calculated by nonlinear regression (Prism ver. 9.0.2, GraphPad Software, San Diego, CA, USA).

Cell viability—The ratio of living to dead cells in a randomly selected 40x field of view (~70–100 cells in view) using a Zeiss confocal laser scanning microscope (LSM 700; see Imaging below; n=3). Data were plotted using GraphPad Prism (Ver. 9.5.0, San Diego, CA, USA) and are presented as mean±SEM. Data was analyzed using one-way ANOVA; significance was demonstrated by surpassing an α level of 0.05.

Dendritogenesis and spinogenesis in cultured neurons—For the dendritogenesis experiment (n=30 cells) and 5-HT_{2A} antagonist experiment (n=25 cells), arbor complexity was measured using the Neurolucida imaging analysis software suite (Neurolucida 360/ Explorer) and analyzed using a Sholl analysis. Spine densities were calculated by quantifying the number of spines per 10 μm segment of a randomly selected dendrite at least 40 μm long (n=15), using the Xen Black image analysis software suite (Zeiss ZEN Microscopy Software). Data were plotted using GraphPad Prism (Ver. 9.5.0, San Diego, CA, USA) and are presented as mean±SEM. Data were analyzed using one-way or two-way ANOVAs, followed by Bonferroni's post hoc tests for post hoc comparisons; significance was demonstrated by surpassing an α level of 0.05.

Spine density (Golgi staining)—Dendritic spine density was quantified manually by counting the number of spines on the longest apical dendrite of randomly selected PFC pyramidal neurons, at least 40 um in length starting from the first branch node (n=5 neurons / n=11 mice / sex). Data were plotted using GraphPad Prism (Ver. 9.5.0, San Diego, CA, USA) and are presented as mean±SEM. Data were analyzed using two-tailed Student's t-test; significance was demonstrated by surpassing an α level of 0.05.

Open field, forced swim test and splash test—OFT videos were processed using DeepLabCut software[111,112] (DLC, version 2.2.1) and custom scripts. Variables quantified included total distance traveled and time in the center of the arena. We tracked the body parts of the mouse using DeepLabCut[111,112] (DLC, version 2.2.1). We used a ResNet50-based model and trained it on a dataset of 288 images with a 95% training/test split. The reported test error across 5 shuffles was 2.95 pixels[113,114]. Outliers were removed by filtering DLC predictions with a confidence less than 0.9. In addition, we also removed body parts that were >3 SD from the mean with regards to movement speed or relative distance to other body parts. Filtered data was filled using linear interpolation.

In order to create the heatmaps, precisely measure distances, and use the same center zone across all videos, we corrected for any differences between camera and test arena location. We performed this correction by identifying the pixel coordinates of the test arena corners in each video and solved for the homogeneous transformation which mapped them to the real measurements of the test arena. The homogeneous transformations could then be applied to the DLC coordinates, transforming them from the camera's frame of reference to the test arena's frame of reference, and from pixel units to mm. Heatmaps, distances, and time in the center area were produced using these transformed coordinates. Smoothing for the heatmaps was done using Gaussian Kernel Density Estimation. The center area of the Open Field Test was defined as being 7cm away from the walls of the box. This center area size was selected by plotting the mouse positions and identifying the largest center area which excluded any clusters near the walls.

All code is available online at: https://github.com/A-Telfer/bapipe-keypoints/tree/fd24e3c7b16bd9901db95f3bbc46efc6f13268f6.

For FST quantification, an experimenter blinded to treatment manually recorded immobility time during the last 4 minutes of the test. Immobility was defined as the animal lacking any lateral movement with not more than one limb moving in full swim rotation, for at least 1 second.

For the ST quantification, self-grooming time was scored for the 10 min period following sucrose application by an experimenter blind to the treatment.

Data were plotted using GraphPad Prism (Ver. 9.5.0, San Diego, CA, USA) and are presented as mean±SEM. Data were analyzed using one-way or two-way ANOVAs, followed by Bonferroni's post hoc tests for post hoc comparisons; significance was demonstrated by surpassing an α level of 0.05.

Supplementary Material

Refer to Web version on PubMed Central for supplementary material.

Acknowledgments

Support from this project came from R35GM133421 to J.D.M. A.A.V. and V.L. were awarded two MITACS accelerate grants for this project (IT27497 and IT24847). We would like to thank Ms. Stephanie Simard, Dr. Natalina Salmaso, Mr. Brendan Hoffe, and Dr. Matthew Holahan for their support while performing the stress and neuronal culture experiments and analyses. Finally, Ms. Sofia Mah, Sumika Egner, and Rebeca Gonzalez Gonzalez assisted the chronic stress experiment.

Inclusion and Diversity

One or more of the authors of this paper self-identifies as an underrepresented ethnic minority in science, self-identifies as a gender minority in their field of research, or self-identifies as living with a disability.

References

1. Kessler RC, Sampson NA, Berglund P, Gruber MJ, Al-Hamzawi A, Andrade L, Bunting B, Demyttenaere K, Florescu S, de Girolamo G, et al. (2015). Anxious and non-anxious major depressive disorder in the World Health Organization World Mental Health Surveys. Epidemiol Psychiatr Sci 24, 210–226. 10.1017/S2045796015000189. [PubMed: 25720357]
2. Kalin NH (2020). The Critical Relationship Between Anxiety and Depression. Am J Psychiatry 177, 365–367. 10.1176/appi.ajp.2020.20030305. [PubMed: 32354270]
3. Lader M (2007). Limitations of current medical treatments for depression: disturbed circadian rhythms as a possible therapeutic target. Eur Neuropsychopharmacol 17, 743–755. 10.1016/j.euroneuro.2007.05.004. [PubMed: 17624740]
4. Frodl T (2017). Recent advances in predicting responses to antidepressant treatment. F1000Res 6. 10.12688/f1000research.10300.1.
5. Hibicke M, Landry AN, Kramer HM, Talman ZK, and Nichols CD (2020). Psychedelics, but Not Ketamine, Produce Persistent Antidepressant-like Effects in a Rodent Experimental System for the Study of Depression. ACS Chem Neurosci 11, 864–871. 10.1021/acschemneuro.9b00493. [PubMed: 32133835]
6. de Vos CMH, Mason NL, and Kuypers KPC (2021). Psychedelics and Neuroplasticity: A Systematic Review Unraveling the Biological Underpinnings of Psychedelics. Front Psychiatry 12, 724606. 10.3389/fpsyt.2021.724606. [PubMed: 34566723]
7. Halberstadt AL (2015). Recent advances in the neuropsychopharmacology of serotonergic hallucinogens. Behav Brain Res 277, 99–120. 10.1016/j.bbr.2014.07.016. [PubMed: 25036425]
8. Nichols DE (2016). Psychedelics. Pharmacol Rev 68, 264–355. 10.1124/pr.115.011478. [PubMed: 26841800]
9. Dos Santos RG, Osorio FL, Crippa JA, Riba J, Zuardi AW, and Hallak JE (2016). Antidepressive, anxiolytic, and antiaddictive effects of ayahuasca, psilocybin and lysergic acid diethylamide (LSD): a systematic review of clinical trials published in the last 25 years. Ther Adv Psychopharmacol 6, 193–213. 10.1177/2045125316638008. [PubMed: 27354908]
10. Carhart-Harris RL, Bolstridge M, Day CMJ, Rucker J, Watts R, Erritzoe DE, Kaelen M, Giribaldi B, Bloomfield M, Pilling S, et al. (2018). Psilocybin with psychological support for treatment-resistant depression: six-month follow-up. Psychopharmacology (Berl) 235, 399–408. 10.1007/s00213-017-4771-x. [PubMed: 29119217]
11. Palhano-Fontes F, Barreto D, Onias H, Andrade KC, Novaes MM, Pessoa JA, Mota-Rolim SA, Osorio FL, Sanches R, Dos Santos RG, et al. (2019). Rapid antidepressant effects of the psychedelic ayahuasca in treatment-resistant depression: a randomized placebo-controlled trial. Psychol Med 49, 655–663. 10.1017/S0033291718001356. [PubMed: 29903051]
12. Kryst J, Kawalec P, Mitoraj AM, Pilc A, Lason W, and Brzostek T (2020). Efficacy of single and repeated administration of ketamine in unipolar and bipolar depression: a meta-analysis of randomized clinical trials. Pharmacol Rep 72, 543–562. 10.1007/s43440-020-00097-z. [PubMed: 32301056]
13. De Gregorio D, Aguilar-Valles A, Preller KH, Heifets BD, Hibicke M, Mitchell J, and Gobbi G (2021). Hallucinogens in Mental Health: Preclinical and Clinical Studies on LSD, Psilocybin, MDMA, and Ketamine. The Journal of neuroscience : the official journal of the Society for Neuroscience 41, 891–900. 10.1523/JNEUROSCI.1659-20.2020. [PubMed: 33257322]
14. Le TT, Cordero IP, Jawad MY, Swainson J, Di Vincenzo JD, Jaberi S, Phan L, Lui LMW, Ho R, Rosenblat JD, and McIntyre RS (2022). The abuse liability of ketamine: A scoping review of preclinical and clinical studies. J Psychiatr Res 151, 476–496. 10.1016/j.jpsychires.2022.04.035. [PubMed: 35623124]
15. Griffiths RR, Johnson MW, Carducci MA, Umbricht A, Richards WA, Richards BD, Cosimano MP, and Klinedinst MA (2016). Psilocybin produces substantial and sustained decreases in depression and anxiety in patients with life-threatening cancer: A randomized double-blind trial. J Psychopharmacol 30, 1181–1197. 10.1177/0269881116675513. [PubMed: 27909165]
16. Ross S, Bossis A, Guss J, Agin-Liebes G, Malone T, Cohen B, Mennenga SE, Belser A, Kalliontzi K, Babb J, et al. (2016). Rapid and sustained symptom reduction following psilocybin treatment

for anxiety and depression in patients with life-threatening cancer: a randomized controlled trial. J Psychopharmacol 30, 1165–1180. 10.1177/0269881116675512. [PubMed: 27909164]

17. Siegel AN, Meshkat S, Benitah K, Lipsitz O, Gill H, Lui LMW, Teopiz KM, McIntyre RS, and Rosenblat JD (2021). Registered clinical studies investigating psychedelic drugs for psychiatric disorders. J Psychiatr Res 139, 71–81. 10.1016/j.jpsychires.2021.05.019. [PubMed: 34048997]
18. Olson DE (2021). The Subjective Effects of Psychedelics May Not Be Necessary for Their Enduring Therapeutic Effects. ACS Pharmacol Transl Sci 4, 563–567. 10.1021/acsptsci.0c00192. [PubMed: 33861218]
19. Yaden DB, and Griffiths RR (2021). The Subjective Effects of Psychedelics Are Necessary for Their Enduring Therapeutic Effects. ACS Pharmacol Transl Sci 4, 568–572. 10.1021/acsptsci.0c00194. [PubMed: 33861219]
20. Stenbaek DS, Madsen MK, Ozenne B, Kristiansen S, Burmester D, Erritzoe D, Knudsen GM, and Fisher PM (2021). Brain serotonin 2A receptor binding predicts subjective temporal and mystical effects of psilocybin in healthy humans. J Psychopharmacol 35, 459–468. 10.1177/0269881120959609. [PubMed: 33501857]
21. Madsen MK, Fisher PM, Burmester D, Dyssegaard A, Stenbaek DS, Kristiansen S, Johansen SS, Lehel S, Linnet K, Svarer C, et al. (2019). Psychedelic effects of psilocybin correlate with serotonin 2A receptor occupancy and plasma psilocin levels. Neuropsychopharmacology 44, 1328–1334. 10.1038/s41386-019-0324-9. [PubMed: 30685771]
22. Hesselgrave N, Troppoli TA, Wulff AB, Cole AB, and Thompson SM (2021). Harnessing psilocybin: antidepressant-like behavioral and synaptic actions of psilocybin are independent of 5-HT2R activation in mice. Proc Natl Acad Sci U S A 118. 10.1073/pnas.2022489118.
23. Price RB, and Duman R (2020). Neuroplasticity in cognitive and psychological mechanisms of depression: an integrative model. Mol Psychiatry 25, 530–543. 10.1038/s41380-019-0615-x. [PubMed: 31801966]
24. Ly C, Greb AC, Vargas MV, Duim WC, Grodzki ACG, Lein PJ, and Olson DE (2021). Transient Stimulation with Psychoplastogens Is Sufficient to Initiate Neuronal Growth. ACS Pharmacol Transl Sci 4, 452–460. 10.1021/acsptsci.0c00065. [PubMed: 33860174]
25. Olson DE (2022). Biochemical Mechanisms Underlying Psychedelic-Induced Neuroplasticity. Biochemistry 61, 127–136. 10.1021/acs.biochem.1c00812. [PubMed: 35060714]
26. Radulescu I, Dragoi AM, Trifu SC, and Cristea MB (2021). Neuroplasticity and depression: Rewiring the brain's networks through pharmacological therapy (Review). Exp Ther Med 22, 1131. 10.3892/etm.2021.10565. [PubMed: 34504581]
27. Cameron LP, Tombari RJ, Lu J, Pell AJ, Hurley ZQ, Ehinger Y, Vargas MV, McCarroll MN, Taylor JC, Myers-Turnbull D, et al. (2021). A non-hallucinogenic psychedelic analogue with therapeutic potential. Nature 589, 474–479. 10.1038/s41586-020-3008-z. [PubMed: 33299186]
28. Stoll A, and Hofmann A (1943). Partialsynthese von Alkaloiden vom Typus des Ergobasins. (6. Mitteilung über Mutterkornalkaloide). Helvetica Chimica Acta 26, 944–965. 10.1002/hlca.19430260326.
29. Smith CM (1959). Some reflections on the possible therapeutic effects of the hallucinogens; with special reference to alcoholism. Quarterly journal of studies on alcohol 20 2, 292–301. [PubMed: 13668045]
30. Bertino JR, Klee GD, and Weintraub W (1959). Cholinesterase, dlysergic acid diethylamide, and 2-bromolysergic acid diethylamide. J Clin Exp Psychopathol Q Rev Psychiatry Neurol 20, 218–222. [PubMed: 13799991]
31. Karst M, Halpern JH, Bernateck M, and Passie T (2010). The non-hallucinogen 2-bromo-lysergic acid diethylamide as preventative treatment for cluster headache: an open, non-randomized case series. Cephalalgia 30, 1140–1144. 10.1177/0333102410363490. [PubMed: 20713566]
32. Sewell RA, Halpern JH, and Pope HG Jr. (2006). Response of cluster headache to psilocybin and LSD. Neurology 66, 1920–1922. 10.1212/01.wnl.0000219761.05466.43. [PubMed: 16801660]
33. Burris KD, and Sanders-Bush E (1992). Unsurmountable antagonism of brain 5-hydroxytryptamine2 receptors by (+)-lysergic acid diethylamide and bromo-lysergic acid diethylamide. Mol Pharmacol 42, 826–830. [PubMed: 1359397]

34. Ginzel KH, and Mayer-Gross W (1956). Prevention of psychological effects of d-lysergic acid diethylamide (LSD 25) by its 2-brom derivative (BOL 148). Nature 178, 210. 10.1038/178210a0.
35. Peng Y, McCorvy JD, Harpsoe K, Lansu K, Yuan S, Popov P, Qu L, Pu M, Che T, Nikolajsen LF, et al. (2018). 5-HT(2C) Receptor Structures Reveal the Structural Basis of GPCR Polypharmacology. Cell 172, 719–730 e714. 10.1016/j.cell.2018.01.001. [PubMed: 29398112]
36. Wacker D, Wang C, Katritch V, Han GW, Huang XP, Vardy E, McCorvy JD, Jiang Y, Chu M, Siu FY, et al. (2013). Structural features for functional selectivity at serotonin receptors. Science 340, 615–619. 10.1126/science.1232808. [PubMed: 23519215]
37. Roth BL, Choudhary MS, Khan N, and Uluer AZ (1997). High-affinity agonist binding is not sufficient for agonist efficacy at 5-hydroxytryptamine2A receptors: evidence in favor of a modified ternary complex model. J Pharmacol Exp Ther 280, 576–583. [PubMed: 9023266]
38. Olsen RHJ, DiBerto JF, English JG, Glaudin AM, Krumm BE, Slocum ST, Che T, Gavin AC, McCorvy JD, Roth BL, and Strachan RT (2020). TRUPATH, an open-source biosensor platform for interrogating the GPCR transducerome. Nat Chem Biol 16, 841–849. 10.1038/s41589-020-0535-8.
39. Wacker D, Wang S, McCorvy JD, Betz RM, Venkatakrishnan AJ, Levit A, Lansu K, Schools ZL, Che T, Nichols DE, et al. (2017). Crystal Structure of an LSD-Bound Human Serotonin Receptor. Cell 168, 377–389 e312. 10.1016/j.cell.2016.12.033. [PubMed: 28129538]
40. Ramirez Rosas MB, Labruijere S, Villalon CM, and Maassen Vandenbrink A (2013). Activation of 5-hydroxytryptamine1B/1D/1F receptors as a mechanism of action of antimigraine drugs. Expert Opin Pharmacother 14, 1599–1610. 10.1517/14656566.2013.806487. [PubMed: 23815106]
41. Drop M, Canale V, Chaumont-Dubel S, Kurczab R, Satala G, Bantreil X, Walczak M, Koczurkiewicz-Adamczyk P, Latacz G, Gwizdak A, et al. (2021). 2-Phenyl-1H-pyrrole-3-carboxamide as a New Scaffold for Developing 5-HT(6) Receptor Inverse Agonists with Cognition-Enhancing Activity. ACS Chem Neurosci 12, 1228–1240. 10.1021/acschemneuro.1c00061. [PubMed: 33705101]
42. Watts VJ, Lawler CP, Fox DR, Neve KA, Nichols DE, and Mailman RB (1995). LSD and structural analogs: pharmacological evaluation at D1 dopamine receptors. Psychopharmacology (Berl) 118, 401–409. 10.1007/BF02245940. [PubMed: 7568626]
43. Preller KH, Herdener M, Pokorny T, Planzer A, Kraehenmann R, Stampfli P, Liechti ME, Seifritz E, and Vollenweider FX (2017). The Fabric of Meaning and Subjective Effects in LSD-Induced States Depend on Serotonin 2A Receptor Activation. Curr Biol 27, 451–457. 10.1016/j.cub.2016.12.030. [PubMed: 28132813]
44. Holze F, Vizeli P, Ley L, Muller F, Dolder P, Stocker M, Duthaler U, Varghese N, Eckert A, Borgwardt S, and Liechti ME (2021). Acute dose-dependent effects of lysergic acid diethylamide in a double-blind placebo-controlled study in healthy subjects. Neuropsychopharmacology 46, 537–544. 10.1038/s41386-020-00883-6. [PubMed: 33059356]
45. Zhang JY, Kowal DM, Nawoschik SP, Lou Z, and Dunlop J (2006). Distinct functional profiles of aripiprazole and olanzapine at RNA edited human 5-HT2C receptor isoforms. Biochem Pharmacol 71, 521–529. 10.1016/j.bcp.2005.11.007. [PubMed: 16336943]
46. Dursun SM, and Handley SL (1996). Similarities in the pharmacology of spontaneous and DOI-induced head-shakes suggest 5HT2A receptors are active under physiological conditions. Psychopharmacology (Berl) 128, 198–205. 10.1007/s002130050125. [PubMed: 8956381]
47. Canal CE, and Morgan D (2012). Head-twitch response in rodents induced by the hallucinogen 2,5-dimethoxy-4-iodoamphetamine: a comprehensive history, a re-evaluation of mechanisms, and its utility as a model. Drug Test Anal 4, 556–576. 10.1002/dta.1333. [PubMed: 22517680]
48. Gonzalez-Maeso J, Weisstaub NV, Zhou M, Chan P, Ivic L, Ang R, Lira A, Bradley-Moore M, Ge Y, Zhou Q, et al. (2007). Hallucinogens recruit specific cortical 5-HT(2A) receptor-mediated signaling pathways to affect behavior. Neuron 53, 439–452. 10.1016/j.neuron.2007.01.008. [PubMed: 17270739]
49. Araneda R, and Andrade R (1991). 5-Hydroxytryptamine2 and 5-hydroxytryptamine 1A receptors mediate opposing responses on membrane excitability in rat association cortex. Neuroscience 40, 399–412. 10.1016/0306-4522(91)90128-b. [PubMed: 1851255]

50. Borroto-Escuela DO, Li X, Tarakanov AO, Savelli D, Narvaez M, Shumilov K, Andrade-Talavera Y, Jimenez-Beristain A, Pomierny B, Diaz-Cabiale Z, et al. (2017). Existence of Brain 5-HT1A-5-HT2A Isoreceptor Complexes with Antagonistic Allosteric Receptor-Receptor Interactions Regulating 5-HT1A Receptor Recognition. ACS Omega 2, 4779–4789. 10.1021/acsomega.7b00629. [PubMed: 28920103]
51. Darmani NA, Martin BR, Pandey U, and Glennon RA (1990). Do functional relationships exist between 5-HT1A and 5-HT2 receptors? Pharmacology Biochemistry and Behavior 36, 901–906. 10.1016/0091-3057(90)90098-3. [PubMed: 2145593]
52. Schreiber R, Brocco M, Audinot V, Gobert A, Veiga S, and Millan MJ (1995). (1-(2,5-dimethoxy-4 iodophenyl)-2-aminopropane)-induced head-twitches in the rat are mediated by 5-hydroxytryptamine (5-HT) 2A receptors: modulation by novel 5-HT2A/2C antagonists, D1 antagonists and 5-HT1A agonists. J Pharmacol Exp Ther 273, 101–112. [PubMed: 7714755]
53. Brandt SD, Kavanagh PV, Twamley B, Westphal F, Elliott SP, Wallach J, Stratford A, Klein LM, McCorvy JD, Nichols DE, and Halberstadt AL (2018). Return of the lysergamides. Part IV: Analytical and pharmacological characterization of lysergic acid morpholide (LSM-775). Drug Test Anal 10, 310–322. 10.1002/dta.2222. [PubMed: 28585392]
54. Rothman RB, and Baumann MH (2009). Serotonergic drugs and valvular heart disease. Expert Opin Drug Saf 8, 317–329. 10.1517/14740330902931524. [PubMed: 19505264]
55. Horvath J, Fross RD, Kleiner-Fisman G, Lerch R, Stalder H, Liaudat S, Raskoff WJ, Flachsbart KD, Rakowski H, Pache JC, et al. (2004). Severe multivalvular heart disease: a new complication of the ergot derivative dopamine agonists. Mov Disord 19, 656–662. 10.1002/mds.20201. [PubMed: 15197703]
56. Hutcheson JD, Setola V, Roth BL, and Merryman WD (2011). Serotonin receptors and heart valve disease--it was meant 2B. Pharmacol Ther 132, 146–157. 10.1016/j.pharmthera.2011.03.008. [PubMed: 21440001]
57. Reiter E, Ahn S, Shukla AK, and Lefkowitz RJ (2012). Molecular mechanism of beta-arrestin-biased agonism at seven-transmembrane receptors. Annu Rev Pharmacol Toxicol 52, 179–197. 10.1146/annurev.pharmtox.010909.105800. [PubMed: 21942629]
58. Tan L, Yan W, McCorvy JD, and Cheng J (2018). Biased Ligands of G Protein-Coupled Receptors (GPCRs): Structure-Functional Selectivity Relationships (SFSRs) and Therapeutic Potential. J Med Chem 61, 9841–9878. 10.1021/acs.jmedchem.8b00435. [PubMed: 29939744]
59. Aguilar-Valles A, De Gregorio D, Matta-Camacho E, Eslamizade MJ, Khlaifia A, Skaleka A, Lopez-Canul M, Torres-Berrio A, Bermudez S, Rurak GM, et al. (2021). Antidepressant actions of ketamine engage cell-specific translation via eIF4E. Nature. 10.1038/s41586-020-03047-0.
60. Moda-Sava RN, Murdock MH, Parekh PK, Fetcho RN, Huang BS, Huynh TN, Witztum J, Shaver DC, Rosenthal DL, Alway EJ, et al. (2019). Sustained rescue of prefrontal circuit dysfunction by antidepressant-induced spine formation. Science 364. 10.1126/science.aat8078.
61. Carhart-Harris RL, Bolstridge M, Rucker J, Day CM, Erritzoe D, Kaelen M, Bloomfield M, Rickard JA, Forbes B, Feilding A, et al. (2016). Psilocybin with psychological support for treatment-resistant depression: an open-label feasibility study. Lancet Psychiatry 3, 619–627. 10.1016/S2215-0366(16)30065-7. [PubMed: 27210031]
62. Buchborn T, Schroder H, Hollt V, and Grecksch G (2014). Repeated lysergic acid diethylamide in an animal model of depression: Normalisation of learning behaviour and hippocampal serotonin 5-HT2 signalling. J Psychopharmacol 28, 545–552. 10.1177/0269881114531666. [PubMed: 24785760]
63. Cameron LP, Benson CJ, DeFelice BC, Fiehn O, and Olson DE (2019). Chronic, Intermittent Microdoses of the Psychedelic N,N-Dimethyltryptamine (DMT) Produce Positive Effects on Mood and Anxiety in Rodents. ACS Chem Neurosci 10, 3261–3270. 10.1021/acschemneuro.8b00692. [PubMed: 30829033]
64. Cameron LP, Benson CJ, Dunlap LE, and Olson DE (2018). Effects of N, N-Dimethyltryptamine on Rat Behaviors Relevant to Anxiety and Depression. ACS Chem Neurosci 9, 1582–1590. 10.1021/acschemneuro.8b00134. [PubMed: 29664276]
65. Harro J (2019). Animal models of depression: pros and cons. Cell Tissue Res 377, 5–20. 10.1007/s00441-018-2973-0. [PubMed: 30560458]

66. Strekalova T, Liu Y, Kiselev D, Khairuddin S, Chiu JLY, Lam J, Chan YS, Pavlov D, Proshin A, Lesch KP, et al. (2022). Chronic mild stress paradigm as a rat model of depression: facts, artifacts, and future perspectives. Psychopharmacology (Berl) 239, 663–693. 10.1007/s00213-021-05982-w. [PubMed: 35072761]

67. Li N, Lee B, Liu RJ, Banasr M, Dwyer JM, Iwata M, Li XY, Aghajanian G, and Duman RS (2010). mTOR-dependent synapse formation underlies the rapid antidepressant effects of NMDA antagonists. Science 329, 959–964. 10.1126/science.1190287. [PubMed: 20724638]

68. Carreno FR, Donegan JJ, Boley AM, Shah A, DeGuzman M, Frazer A, and Lodge DJ (2016). Activation of a ventral hippocampus-medial prefrontal cortex pathway is both necessary and sufficient for an antidepressant response to ketamine. Mol Psychiatry 21, 1298–1308. 10.1038/mp.2015.176. [PubMed: 26619811]

69. Gerhard DM, Pothula S, Liu RJ, Wu M, Li XY, Girgenti MJ, Taylor SR, Duman CH, Delpire E, Picciotto M, et al. (2020). GABA interneurons are the cellular trigger for ketamine's rapid antidepressant actions. J Clin Invest 130, 1336–1349. 10.1172/JCI130808. [PubMed: 31743111]

70. Fogaca MV, Wu M, Li C, Li XY, Picciotto MR, and Duman RS (2021). Inhibition of GABA interneurons in the mPFC is sufficient and necessary for rapid antidepressant responses. Mol Psychiatry 26, 3277–3291. 10.1038/s41380-020-00916-y. [PubMed: 33070149]

71. Warden MR, Selimbeyoglu A, Mirzabekov JJ, Lo M, Thompson KR, Kim SY, Adhikari A, Tye KM, Frank LM, and Deisseroth K (2012). A prefrontal cortex-brainstem neuronal projection that controls response to behavioural challenge. Nature 492, 428–432. 10.1038/nature11617. [PubMed: 23160494]

72. Aguilar-Valles A, Haji N, De Gregorio D, Matta-Camacho E, Eslamizade MJ, Popic J, Sharma V, Cao R, Rummel C, Tanti A, et al. (2018). Translational control of depression-like behavior via phosphorylation of eukaryotic translation initiation factor 4E. Nature communications 9, 2459. 10.1038/s41467-018-04883-5.

73. Checkley S (1996). The neuroendocrinology of depression and chronic stress. Br Med Bull 52, 597–617. 10.1093/oxfordjournals.bmb.a011570. [PubMed: 8949260]

74. Lupien SJ, Juster RP, Raymond C, and Marin MF (2018). The effects of chronic stress on the human brain: From neurotoxicity, to vulnerability, to opportunity. Front Neuroendocrinol 49, 91–105. 10.1016/j.yfrne.2018.02.001. [PubMed: 29421159]

75. Akil H, Gordon J, Hen R, Javitch J, Mayberg H, McEwen B, Meaney MJ, and Nestler EJ (2018). Treatment resistant depression: A multi-scale, systems biology approach. Neurosci Biobehav Rev 84, 272–288. 10.1016/j.neubiorev.2017.08.019. [PubMed: 28859997]

76. Cathomas F, Murrough JW, Nestler EJ, Han MH, and Russo SJ (2019). Neurobiology of Resilience: Interface Between Mind and Body. Biol Psychiatry 86, 410–420. 10.1016/j.biopsych.2019.04.011. [PubMed: 31178098]

77. Inserra A, De Gregorio D, and Gobbi G (2021). Psychedelics in Psychiatry: Neuroplastic, Immunomodulatory, and Neurotransmitter Mechanisms. Pharmacol Rev 73, 202–277. 10.1124/pharmrev.120.000056. [PubMed: 33328244]

78. De Gregorio D, Inserra A, Enns JP, Markopoulos A, Pileggi M, El Rahimy Y, Lopez-Canul M, Comai S, and Gobbi G (2022). Repeated lysergic acid diethylamide (LSD) reverses stress-induced anxiety-like behavior, cortical synaptogenesis deficits and serotonergic neurotransmission decline. Neuropsychopharmacology 47, 1188–1198. 10.1038/s41386-022-01301-9. [PubMed: 35301424]

79. Simard S, Coppola G, Rudyk CA, Hayley S, McQuaid RJ, and Salmaso N (2018). Profiling changes in cortical astroglial cells following chronic stress. Neuropsychopharmacology 43, 1961–1971. 10.1038/s41386-018-0105-x. [PubMed: 29907879]

80. Planchez B, Surget A, and Belzung C (2019). Animal models of major depression: drawbacks and challenges. J Neural Transm (Vienna) 126, 1383–1408. 10.1007/s00702-019-02084-y. [PubMed: 31584111]

81. Halberstadt AL, Chatha M, Klein AK, Wallach J, and Brandt SD (2020). Correlation between the potency of hallucinogens in the mouse head-twitch response assay and their behavioral and subjective effects in other species. Neuropharmacology 167, 107933. 10.1016/j.neuropharm.2019.107933. [PubMed: 31917152]

82. Halberstadt AL, and Geyer MA (2013). Characterization of the head-twitch response induced by hallucinogens in mice: detection of the behavior based on the dynamics of head movement. Psychopharmacology (Berl) 227, 727–739. 10.1007/s00213-013-3006-z. [PubMed: 23407781]
83. Klein AK, Chatha M, Laskowski LJ, Anderson EI, Brandt SD, Chapman SJ, McCorvy JD, and Halberstadt AL (2021). Investigation of the Structure-Activity Relationships of Psilocybin Analogues. ACS Pharmacol Transl Sci 4, 533–542. 10.1021/acsptsci.0c00176. [PubMed: 33860183]
84. Vickers SP, Easton N, Malcolm CS, Allen NH, Porter RH, Bickerdike MJ, and Kennett GA (2001). Modulation of 5-HT(2A) receptor-mediated head-twitch behaviour in the rat by 5-HT(2C) receptor agonists. Pharmacol Biochem Behav 69, 643–652. 10.1016/s0091-3057(01)00552-4. [PubMed: 11509227]
85. Isbell H, Miner EJ, and Logan CR (1959). Cross tolerance between D-2-brom-lysergic acid diethylamide (BOL-148) and the D-diethylamide of lysergic acid (LSD-25). Psychopharmacologia 1, 109–116. 10.1007/BF00409110. [PubMed: 14405871]
86. Isbell H, Miner EJ, and Logan CR (1959). Relationships of psychotomimetic to anti-serotonin potencies of congeners of lysergic acid diethylamide (LSD-25). Psychopharmacologia 1, 20–28. 10.1007/BF00408108. [PubMed: 14405872]
87. Schneckloth R, Page IH, Del Greco F, and Corcoran AC (1957). Effects of serotonin antagonists in normal subjects and patients with carcinoid tumors. Circulation 16, 523–532. 10.1161/01.cir.16.4.523. [PubMed: 13461260]
88. Buckholtz NS, Zhou DF, Freedman DX, and Potter WZ (1990). Lysergic acid diethylamide (LSD) administration selectively downregulates serotonin2 receptors in rat brain. Neuropsychopharmacology 3, 137–148. [PubMed: 1969270]
89. Buckholtz NS, Freedman DX, and Middaugh LD (1985). Daily LSD administration selectively decreases serotonin2 receptor binding in rat brain. Eur J Pharmacol 109, 421–425. 10.1016/0014-2999(85)90407-8. [PubMed: 3987809]
90. Smith RL, Barrett RJ, and Sanders-Bush E (1999). Mechanism of tolerance development to 2,5-dimethoxy-4-iodoamphetamine in rats: down-regulation of the 5-HT2A, but not 5-HT2C, receptor. Psychopharmacology (Berl) 144, 248–254. 10.1007/s002130051000. [PubMed: 10435391]
91. Gresch PJ, Smith RL, Barrett RJ, and Sanders-Bush E (2005). Behavioral tolerance to lysergic acid diethylamide is associated with reduced serotonin-2A receptor signaling in rat cortex. Neuropsychopharmacology 30, 1693–1702. 10.1038/sj.npp.1300711. [PubMed: 15756304]
92. Isbell H, Wolbach AB, Wikler A, and Miner EJ (1961). Cross tolerance between LSD and psilocybin. Psychopharmacologia 2, 147–159. 10.1007/BF00407974. [PubMed: 13717955]
93. Wolbach AB Jr., Isbell H, and Miner EJ (1962). Cross tolerance between mescaline and LSD-25, with a comparison of the mescaline and LSD reactions. Psychopharmacologia 3, 1–14. 10.1007/BF00413101. [PubMed: 14007904]
94. Gelber EI, Kroeze WK, Willins DL, Gray JA, Sinar CA, Hyde EG, Gurevich V, Benovic J, and Roth BL (1999). Structure and function of the third intracellular loop of the 5-hydroxytryptamine2A receptor: the third intracellular loop is alpha-helical and binds purified arrestins. J Neurochem 72, 2206–2214. 10.1046/j.1471-4159.1999.0722206.x. [PubMed: 10217304]
95. de la Fuente Revenga M, Jaster AM, McGinn J, Silva G, Saha S, and Gonzalez-Maeso J (2022). Tolerance and Cross-Tolerance among Psychedelic and Nonpsychedelic 5-HT(2A) Receptor Agonists in Mice. ACS Chem Neurosci 13, 2436–2448. 10.1021/acschemneuro.2c00170. [PubMed: 35900876]
96. Raehal KM, Walker JK, and Bohn LM (2005). Morphine side effects in beta-arrestin 2 knockout mice. J Pharmacol Exp Ther 314, 1195–1201. 10.1124/jpet.105.087254. [PubMed: 15917400]
97. Kliewer A, Gillis A, Hill R, Schmiedel F, Bailey C, Kelly E, Henderson G, Christie MJ, and Schulz S (2020). Morphine-induced respiratory depression is independent of beta-arrestin2 signalling. Br J Pharmacol 177, 2923–2931. 10.1111/bph.15004. [PubMed: 32052419]
98. Bachmutsky I, Wei XP, Durand A, and Yackle K (2021). ss-arrestin 2 germline knockout does not attenuate opioid respiratory depression. Elife 10. 10.7554/eLife.62552.

99. Grob CS, Danforth AL, Chopra GS, Hagerty M, McKay CR, Halberstadt AL, and Greer GR (2011). Pilot study of psilocybin treatment for anxiety in patients with advanced-stage cancer. Arch Gen Psychiatry 68, 71–78. 10.1001/archgenpsychiatry.2010.116. [PubMed: 20819978]
100. Wingenfeld K, and Wolf OT (2014). Stress, memory, and the hippocampus. Front Neurol Neurosci 34, 109–120. 10.1159/000356423. [PubMed: 24777135]
101. Ly C, Greb AC, Cameron LP, Wong JM, Barragan EV, Wilson PC, Burbach KF, Soltanzadeh Zarandi S, Sood A, Paddy MR, et al. (2018). Psychedelics Promote Structural and Functional Neural Plasticity. Cell reports 23, 3170–3182. 10.1016/j.celrep.2018.05.022. [PubMed: 29898390]
102. Morales-Garcia JA, Calleja-Conde J, Lopez-Moreno JA, Alonso-Gil S, Sanz-SanCristobal M, Riba J, and Perez-Castillo A (2020). N,N-dimethyltryptamine compound found in the hallucinogenic tea ayahuasca, regulates adult neurogenesis in vitro and in vivo. Transl Psychiatry 10, 331. 10.1038/s41398-020-01011-0. [PubMed: 32989216]
103. Banasr M, Dwyer JM, and Duman RS (2011). Cell atrophy and loss in depression: reversal by antidepressant treatment. Curr Opin Cell Biol 23, 730–737. 10.1016/j.ceb.2011.09.002. [PubMed: 21996102]
104. Carvalho C, Herrmann K, Marques TA, and Knight A (2021). Time to Abolish the Forced Swim Test in Rats for Depression Research? Journal of Applied Animal Ethics Research 4, 170–178. 10.1163/25889567-bja10026.
105. Commons KG, Cholanians AB, Babb JA, and Ehlinger DG (2017). The Rodent Forced Swim Test Measures Stress-Coping Strategy, Not Depression-like Behavior. ACS Chem Neurosci 8, 955–960. 10.1021/acschemneuro.7b00042. [PubMed: 28287253]
106. Kara NZ, Stukalin Y, and Einat H (2018). Revisiting the validity of the mouse forced swim test: Systematic review and meta-analysis of the effects of prototypic antidepressants. Neurosci Biobehav Rev 84, 1–11. 10.1016/j.neubiorev.2017.11.003. [PubMed: 29128579]
107. Willner P (2017). The chronic mild stress (CMS) model of depression: History, evaluation and usage. Neurobiol Stress 6, 78–93. 10.1016/j.ynstr.2016.08.002. [PubMed: 28229111]
108. Kroeze WK, Sassano MF, Huang XP, Lansu K, McCorvy JD, Giguere PM, Sciaky N, and Roth BL (2015). PRESTO-Tango as an open-source resource for interrogation of the druggable human GPCRome. Nat Struct Mol Biol 22, 362–369. 10.1038/nsmb.3014. [PubMed: 25895059]
109. Cheng HC (2001). The power issue: determination of KB or Ki from IC50. A closer look at the Cheng-Prusoff equation, the Schild plot and related power equations. J Pharmacol Toxicol Methods 46, 61–71. 10.1016/s1056-8719(02)00166-1. [PubMed: 12481843]
110. Halberstadt AL (2020). Automated detection of the head-twitch response using wavelet scalograms and a deep convolutional neural network. Sci Rep 10, 8344. 10.1038/s41598-020-65264-x. [PubMed: 32433580]
111. Mathis A, Mamidanna P, Cury KM, Abe T, Murthy VN, Mathis MW, and Bethge M (2018). DeepLabCut: markerless pose estimation of user-defined body parts with deep learning. Nat Neurosci 21, 1281–1289. 10.1038/s41593-018-0209-y. [PubMed: 30127430]
112. Nath T, Mathis A, Chen AC, Patel A, Bethge M, and Mathis MW (2019). Using DeepLabCut for 3D markerless pose estimation across species and behaviors. Nature protocols 14, 2152–2176. 10.1038/s41596-019-0176-0. [PubMed: 31227823]
113. He K, Zhang X, Ren S, and Sun J (2016). Deep Residual Learning for Image Recognition. 27–30 June 2016. pp. 770–778.
114. Insafutdinov E, Pishchulin L, Andres B, Andriluka M, and Schiele B (2016). DeeperCut: A Deeper, Stronger, and Faster Multi-person Pose Estimation Model.

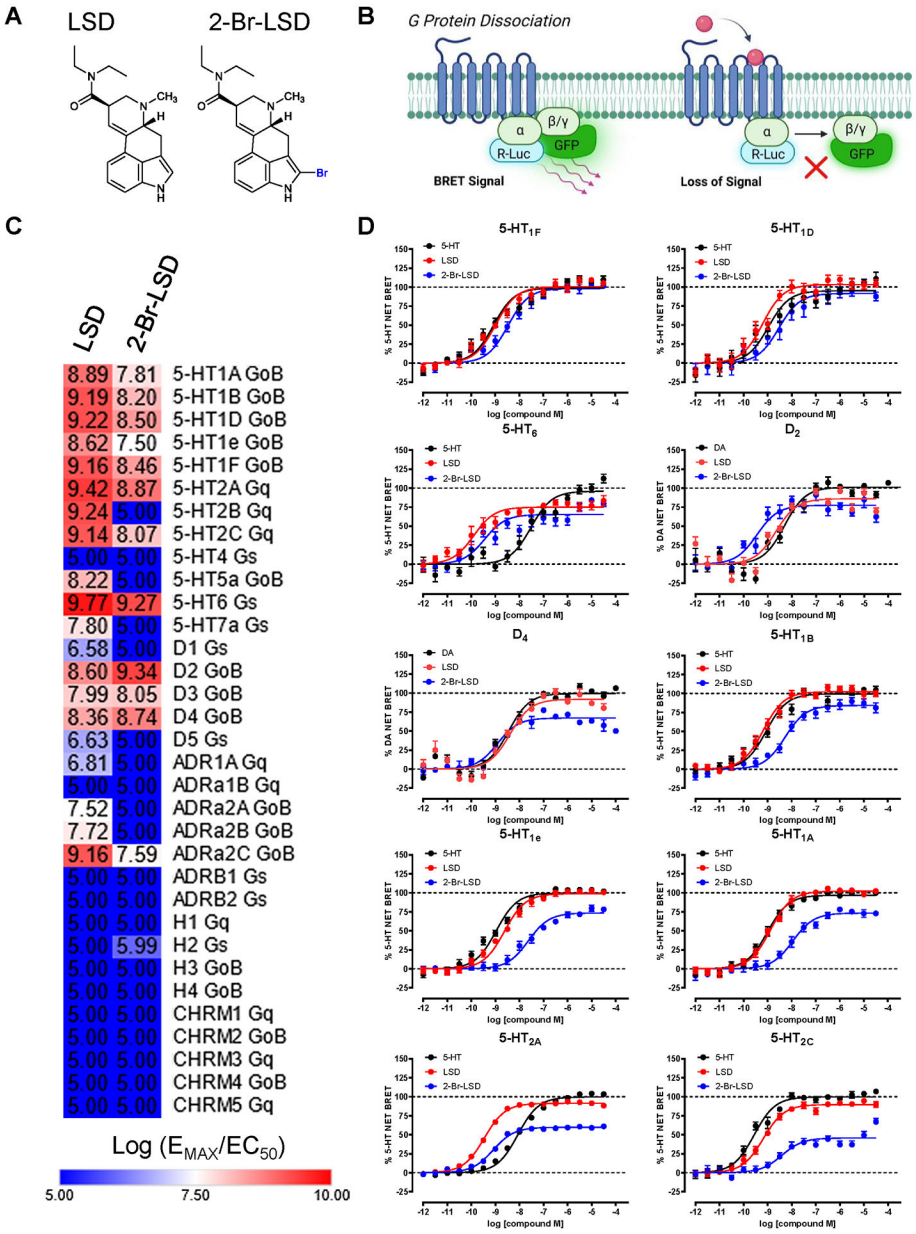

Figure 1. Profiling 2-Br-LSD across the Serotonergic and Aminergic GPCRome

(A) Chemical structures of LSD and 2-Br-LSD. (B) Aminergic-ome G protein dissociation BRET assay schematic. (C) Heat map showing relative agonist activity (log(E_{MAX}/EC_{50}) comparing LSD to 2-Br-LSD at 33 aminergic GPCR targets measuring G protein dissociation at 37°C and 60 minutes (see Table S1). (D) Top ten targets of 2-Br-LSD agonist activity in the BRET aminergic GPCRome activity assays comparing 2-Br-LSD (blue) to LSD (red) and positive control (black; 5-HT for serotonin receptors and DA for dopamine receptors). Data represent mean ± SEM from at least n=3 independent experiments performed in triplicate, and are all normalized to their respective positive control. Related to Fig. S1, S2 and Tables S1–S3.

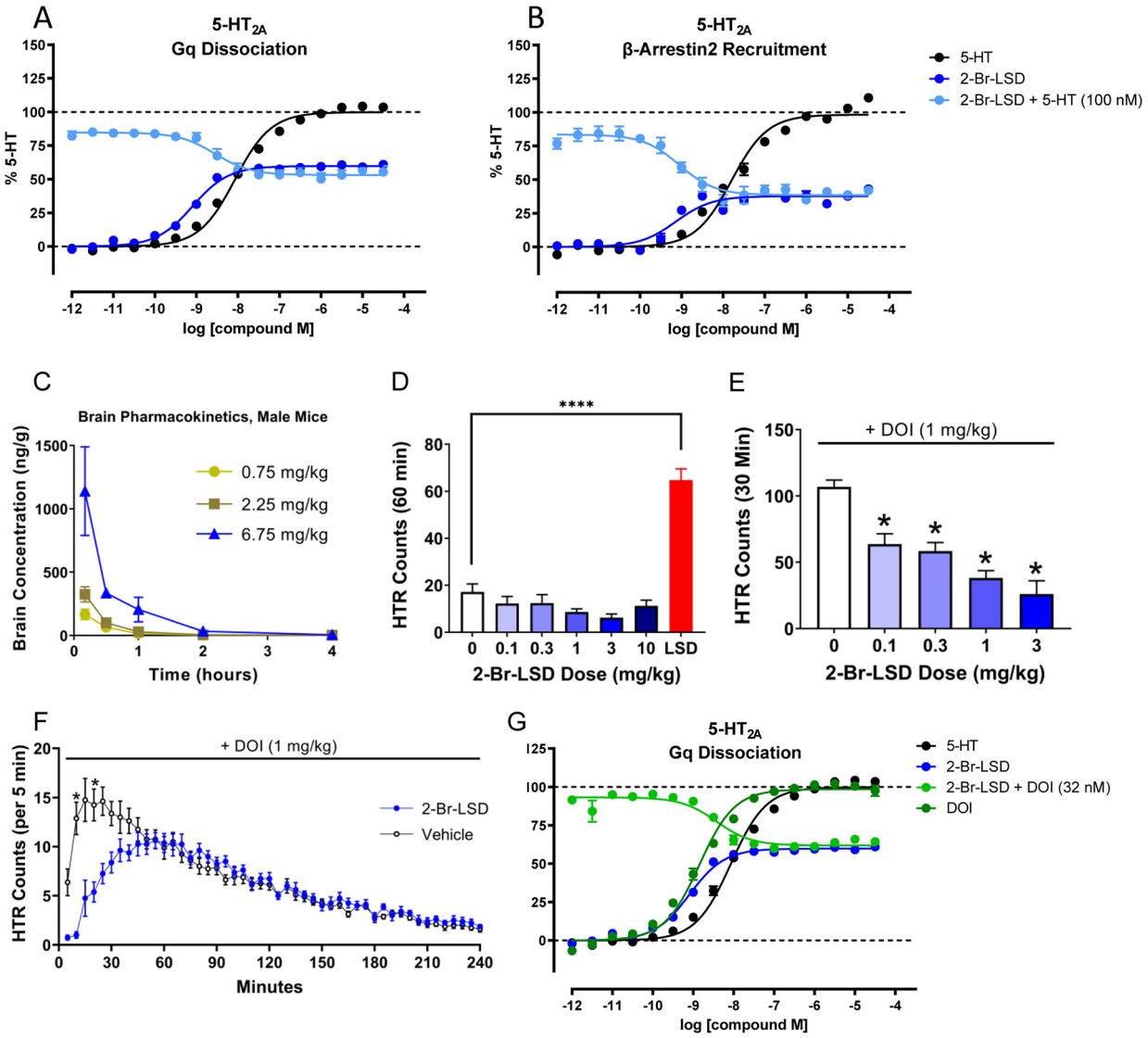

Figure 2. 2-Br-LSD 5-HT$_{2A}$ partial agonist activity, pharmacokinetics, and effect on the head-twitch response (HTR)

2-Br-LSD partial agonist and antagonist activity at 5-HT$_{2A}$ measuring Gq dissociation (A) and β-arrestin2 recruitment (B) in BRET assays. Data represent mean ± SEM from at least n=3 independent experiments performed in triplicate. Antagonist activity K_B was calculated using IC$_{50}$, 5-HT competing concentration, and 5-HT EC$_{50}$. (C) Brain concentration-time curves for 2-Br-LSD in male mice. Data are presented as group means ± SEM. 2-Br-LSD was injected at $t = 0$. (D) Comparison of the effect of different doses of 2-Br-LSD and LSD (0.1 mg/kg IP, n=5–6/group) on the HTR. Data are presented as group means and SEM over the entire 60-minute test session. ****p<0.0001, significant difference between groups (unpaired t-test). (E) Effect of pretreatment with 2-Br-LSD on the HTR induced by DOI. Mice were pretreated IP with vehicle or 2-Br-LSD (n=6–7/group); 10 minutes later, all mice were treated IP with 1 mg/kg DOI and then HTR activity was recorded. Data are presented as group means and SEM over the entire 30-minute test session. *p<0.01, **p<0.001, ***p<0.0001, significant difference vs. vehicle control (Dunnett's test). (F) Time-course of

the interaction between 2-Br-LSD and DOI in the HTR paradigm. Mice were pretreated IP with vehicle (n=8) or 2-Br-LSD (1 mg/kg, n=8); 10 minutes later, all mice were treated IP with 1 mg/kg DOI and then HTR activity was recorded. Data are presented as group means ± SEM during consecutive 5-minute time blocks. *p<0.05, significant difference between groups (Sidak's test). (G) Partial antagonism of 2-Br-LSD, assessed by measuring DOI-induced 5-HT_{2A} Gq dissociation in BRET assays. Antagonist activity K_B was calculated using IC_{50}, DOI competing concentration, and EC_{50}. Data represent mean ± SEM from at least n=3 independent experiments performed in triplicate. Related to Fig. S3 and Table S4.

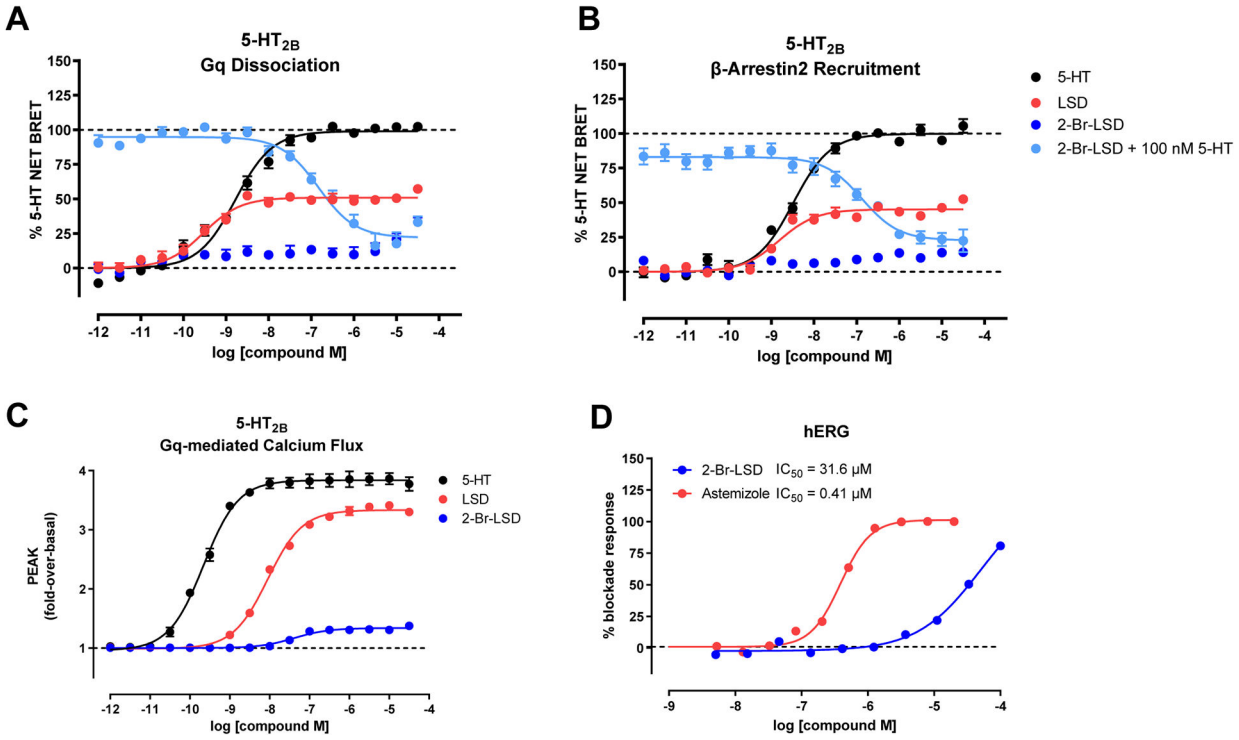

Figure 3. 2-Br-LSD has a safer cardiovascular profile compared to LSD

2-Br-LSD agonist and antagonist activity at 5-HT_{2B} measuring Gq dissociation (A) and β-arrestin2 recruitment (B) in BRET assays, and in Gq-mediated calcium flux assays (C). Data represent mean and SEM from at least n=3 independent experiments performed in triplicate. Antagonist activity K_B was calculated using, IC_{50}, 5-HT competing concentration and EC_{50}. (D) hERG inhibition by 2-Br-LSD (blue) indicating IC_{50} (half maximal inhibition) of 31.6 μM. Positive control astemizole (red) IC_{50} = 0.41 μM. Related to Tables S5, S6.

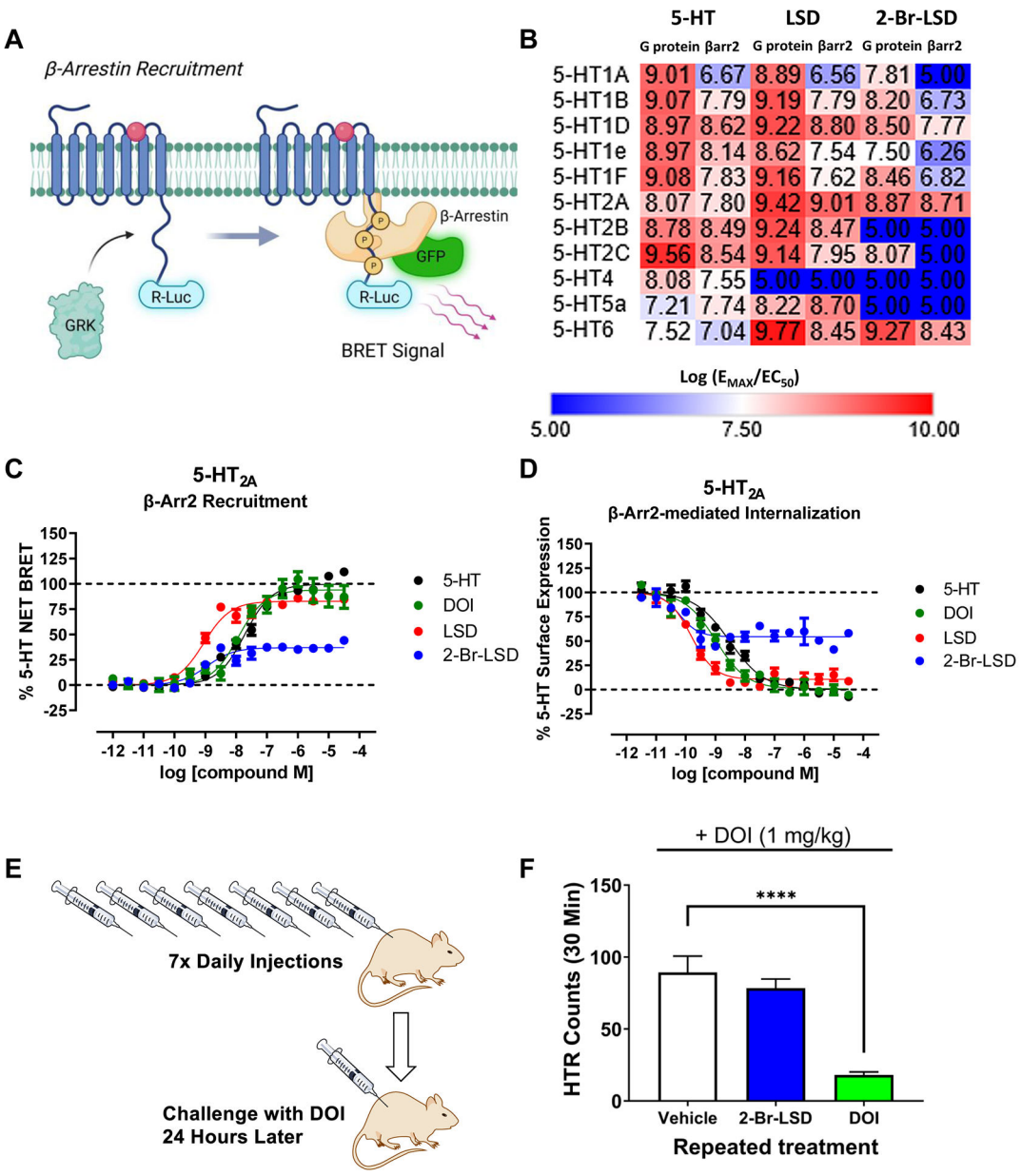

Figure 4. 2-Br-LSD produces weak 5-HT$_{2A}$ β-arrestin recruitment and has reduced potential to induce tolerance *in vivo*

(A) 5-HT-ome β-arrestin2 recruitment BRET assay schematic. (B) Heat map showing relative activity (log(E_{MAX}/EC_{50}) comparing 2-Br-LSD to LSD and 5-HT. (C) Graphs of β-arrestin2 recruitment of 2-Br-LSD (blue) to LSD (red), DOI (green) and 5-HT (black) as measured in the β-arr2 recruitment BRET assay. (D) Graphs of loss of surface expression of 2-Br-LSD (blue) to LSD (red), DOI (green) and 5-HT (black) as measured in NanoBit internalization assay. Data represent mean ± SEM from at least n=3 independent experiments performed in triplicate normalized to percent 5-HT response. (E,F) Lack of tolerance to a 5-HT$_{2A}$ agonist after repeated treatment with 2-Br-LSD. Mice were injected IP once per day with vehicle (n=7), 2-Br-LSD (3 mg/kg, n=7), or DOI (10 mg/kg, n=7) for 7 consecutive days and then challenged with DOI (1 mg/kg IP) 24 hours after the last

injection. Data are presented as group means ± SEM over the entire 30-minute test session. ****p<0.0001, significant difference between groups (Dunnett's test). Related to Fig. S4.

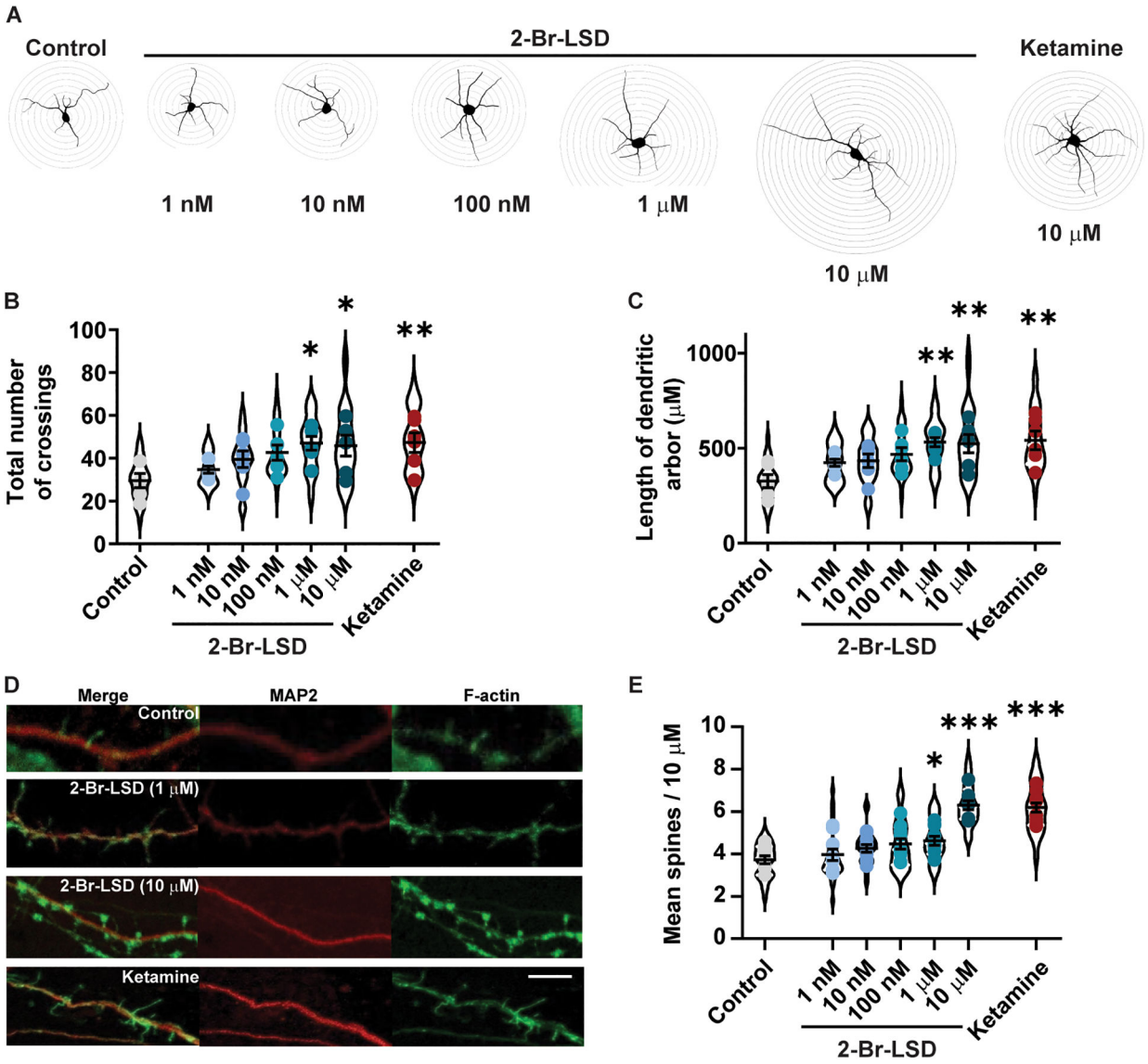

Figure 5. 2-Br-LSD treatment increases dendritic arbour complexity and spine growth in rat cortical pyramidal primary neurons.

(A) Representative Sholl tracings of primary neuronal cultures treated at day *in vitro* (DIV) 3 with 2-Br-LSD (1, 10, 100 nM or 1, 10 μM) or ketamine (10 μM) for 3 h. Then, dendrites were identified by MAP2 staining at DIV 6 and arbor complexity was assessed by Sholl analysis (distance between each Sholl radii is 10 μm). (B) The total number of Sholl radii crossings by MAP2 positive neurites following 2-Br-LSD or ketamine treatment to rat cortical neurons (as described in A), compared to the vehicle control. Violin plots represent the distribution of total crossings by individual neurons (n=30/treatment), and points represent the averages per independent experiment (n=6/treatment). (C) Total dendritic arbor length from neurons from A and B. (D) Representative images of dendritic spines in rat cortical neurons treated with 2-Br-LSD or ketamine (concentrations as in A) at DIV 18 (3 h). Dendrites were imaged at DIV 19 using a combination of F-Actin staining (using phalloidin; green; right panels) and anti-MAP2 antibody (red, center panels), merged

image is in the right panels. Scale bar = 3 μm. (E) The total number of spines per 10 μm section of the longest apical dendrite was scored starting from the first branch point. Violin plots represent average spine density per neuron (n=15/treatment), and points represent averages by independent experiment (n=10/treatment). Horizontal lines represent the mean ± SEM. *p<0.05, **p<0.01 and ***p<0.001 Bonferroni's test vs. control (vehicle-treated neurons). Related to Fig. S5.

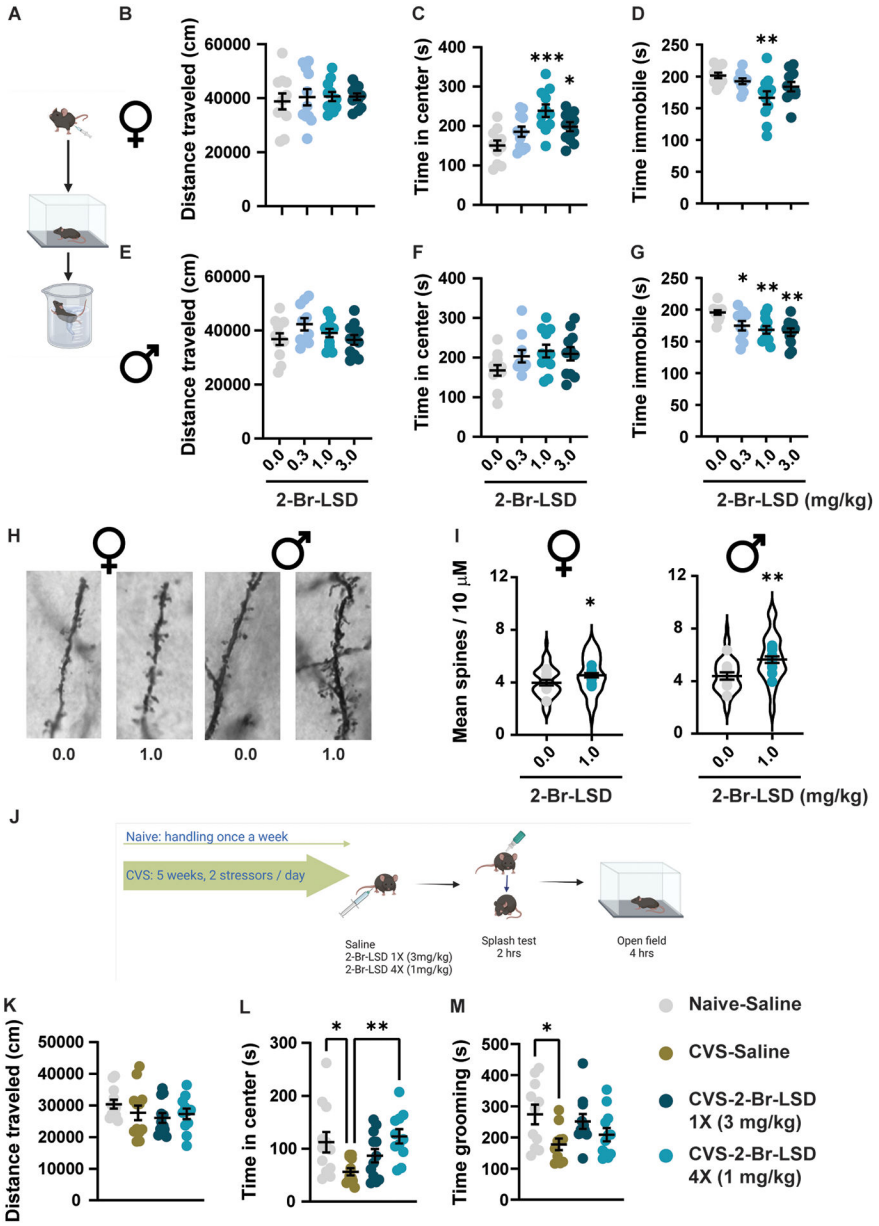

Figure 6. 2-Br-LSD promotes exploration, active coping and spinogenesis in mice.

(A) Female and male mice (n=10–11/group/sex) were treated with 2-Br-LSD (0.3, 1 or 3 mg/kg IP) or vehicle. 24 hrs after injection, mice were tested in the open field and, one hour later, in the forced swim test. (B) and (E) Total distance travelled in the open field, 24 hrs after vehicle or 2-Br-LSD treatment in female and male mice, respectively. (C) and (F) Time in the center of the open field by female and male mice. (D) and (G) Time immobile during the last four minutes in the forced swim test in female and male mice. (H) Representative light microscopy images of dendritic segments of pyramidal neurons of the prefrontal cortex stained using Golgi-Cox. Male and female mice were treated with vehicle or 2-Br-LSD (1 mg/kg IP). (I) Mean spine density per 10 µm dendrite segments in female (left panel) and male (right panel) mice treated with vehicle or 2-Br-LSD. The violin plots

represent the distribution of spine density averages per neuron (Four 10-μm segments per neuron, 5–6 neurons per mouse, 55–60 neurons/treatment/sex). Dots represent the average spine density per mouse (n=10–11 mice/treatment/sex). (J) Female mice were subjected to 5 weeks of chronic variable stress (CSV), consisting of 2 different stressors per day presented randomly. At day 28, after the beginning of the stress, mice were injected IP with vehicle or 2-Br-LSD every 48 h until day 34, so 3 groups were generated: CVS-Saline (4X saline injections), CVS-2-Br-LSD 1X (3 mg/kg) (3 saline injections and one dose of 2-Br-LSD) and CVS-2-Br-LSD 4X (1 mg/kg) (4 doses of 2-Br-LSD). A group of female mice were single-housed and left without manipulation, except for 4 saline injections on the same days as the other groups (Naïve-Saline). Mice were then tested in the splash test and the open field, 2 and 4 h after the last injection). (K) Distance travelled in the open field by female mice treated as described in J (n=12/group). (L) Time spent in the center of the open field of mice in K. (M) Time spent self-grooming in the splash test by female mice treated as in J (n=10–12/group). Horizontal lines represent the mean ± SEM. *$p<0.05$, **$p<0.01$ and ***$p<0.001$ Bonferroni's test vs. control or vs. CVS-Saline mice. Related to Fig. S5 and S6.

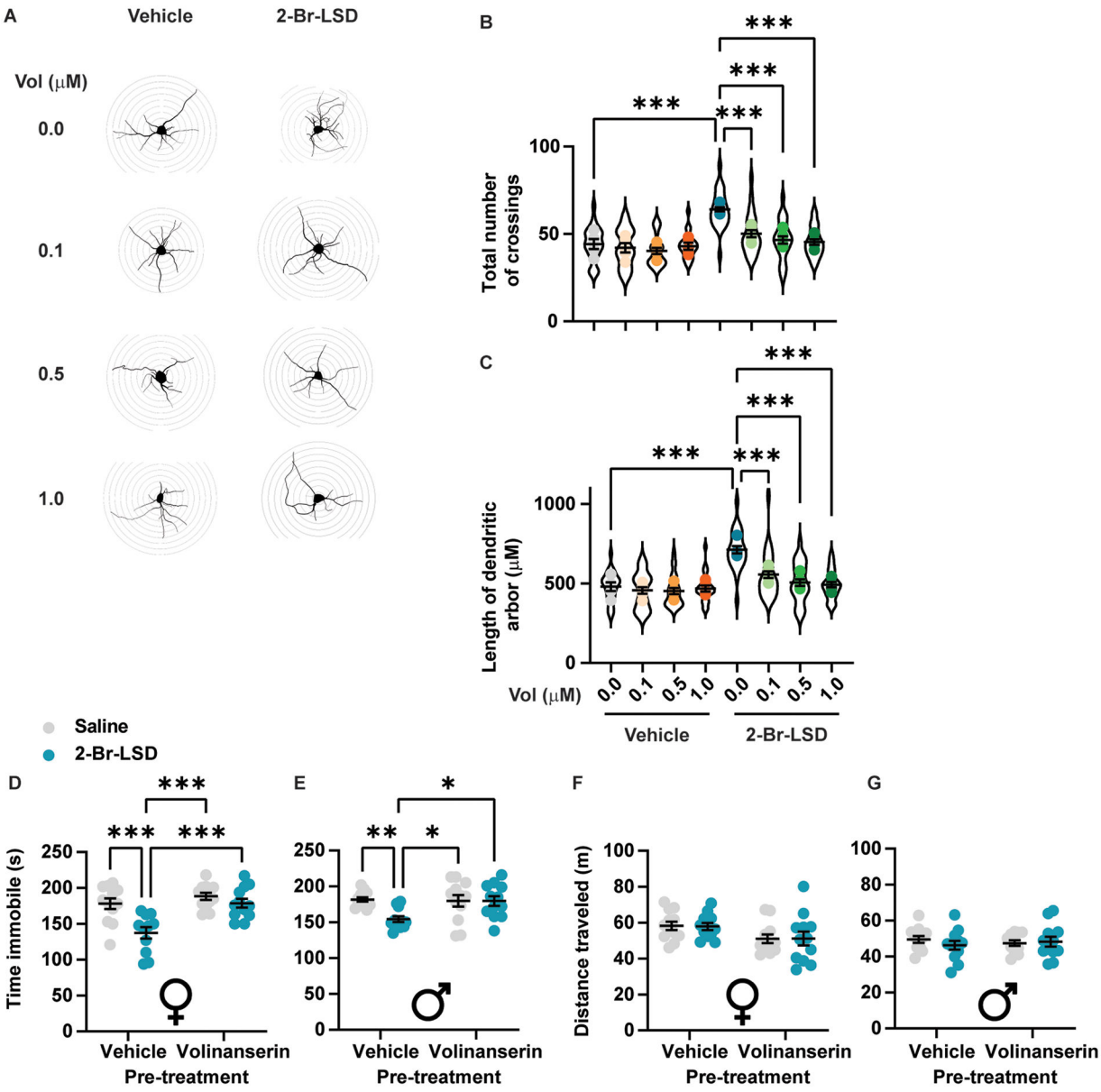

Figure 7. 2-Br-LSD mechanism of action involves 5-HT$_{2A}$ receptor activation.

(A) Representative tracings of primary rat cortical neurons (DIV 3) treated with the selective 5-HT$_{2A}$ antagonist volinanserin (Vol) at 0.1, 0.5 or 1 μM, followed by either vehicle or 2-Br-LSD (1 μM). Sholl radii are spaced 10 μm. (B) Total number of Sholl crossings for neurons treated as in A. (C) Total dendritic arbour length for neurons treated as in A. For both B and C, violin plot represents the distribution of individual cells (n=15/treatment), while dots represent the averages per independent experiment (n=5/treatment). (D) Female mice were pretreated with vehicle or Vol (0.125 mg/kg), followed by either vehicle or 2-Br-LSD (1 mg/kg). Immobility in the FST was measured 25 h after the second injection (n=11–12/group). (E) Male mice were treated as in D and measured for immobility in the FST (n=12/group). (F) Distance travelled in the open field was measured 24 h after treatments in D for female mice. (G) Distance travelled in the open field was measured 24

h after treatments in D for male mice (n=12). Horizontal lines represent the mean ± SEM. *p<0.05, **p<0.01 and ***p<0.001 Bonferroni's test vs. the indicated group. Related to Fig. S6.

KEY RESOURCES TABLE

REAGENT or RESOURCE	SOURCE	IDENTIFIER
Antibodies		
Chicken polyclonal anti-MAP2 antibody	EnCor Biotechnology Inc	Cat#7377–062921
Goat anti-chicken IgY (H+L) secondary antibody, Alexa Fluor 594	Invitrogen	A32759
Phalloidin: Alexa Fluor 488	ThermoFisher Scientific	A12379
anti-FLAG HRP Antibody	Sigma	A8592
Chemicals, peptides, and recombinant proteins		
2-Br-LSD hemitartrate	BetterLife	E559/BETR-001 (Lot# 08-PS-020–2A)
LSD	Sigma-Aldrich	L-001-1ML
(+)-LSD hemitartrate	NIDA Drug Supply	Cat#7315–004
LSD-d3	Sigma-Aldrich	L-002
(5-HT) Serotonin Creatinine Sulfate Monohydrate	Sigma-Aldrich	H7752–500MG
Dopamine	Sigma	H8502–5G
L-(−)-norepinephrine	Cayman Chemical	Cat#16673
(−) Epinephrine	Cayman Chemical	Cat#18626
Pilocarpine	Cayman Chemical	Cat#14487
Histamine	Cayman Chemical	Cat#33828
Volinanserin (M100,907)	Cayman Chemical	Cat#15936
Ketamine hydrochloride	Bimeda Canada	Cat#7087
S-(−)-Raclopride (+)-tartrate	Sigma	R121
(−)-Quinpirole hydrochloride	Sigma	Q102
Ketaset	Zoetis	Cat#10004027
Xylazine	Covetrus	Cat#061035
Meloxicam	Covetrus	Cat#049756
Xylene	Supelco	Cat#1330–20-7
(±)-2,5-dimethoxy-4-iodoamphetamine (DOI) hydrochloride	Cayman Chemical	Cat#13885
Acetronitrile (HPLC grade)	Caledon	Cat#1401–7
Ammonium hydroxide (ACS grade)	Caledon	Cat#1525–1
Methanol (HPLC grade)	Caledon	Cat#6701–7
Poly-L-lysine	Sigma	P2636
Tetracycline	Sigma	T7660
Polyethyleneimine (PEI) solution	Sigma	P3143
Penicillin Streptomycin Solution	VWR	Cat#45000–652
Hygromycin B	Goldbio.com	H-270–1
Blasticidin S HCl	GoldBio	B-800–1
Zeocin	Invitrogen	R25005
DMEM	VWR	Cat#45000–306
FBS	VWR	Cat#97068–085

REAGENT or RESOURCE	SOURCE	IDENTIFIER
Dialyzed FBS	Omega Scientific	FB-03
10xHBSS	Invitrogen	Cat#14065–056
TransIT-2020 Transfection Reagent	VWR	Cat#10766–852
BSA-fatty acid free	Akron	AK8909–0100
10xHBSS	ThermoFisher Scientific	H9394–1L
1 M HEPES	Gibco	Cat#15630080
1 % penicillin-streptomycin	Gibco	Cat#15140122
TrypLE Express	Gibco	Cat#120605–010
Poly-D-lysine	Gibco	A3890401
0.5 mM Glutamax	Gibco	Cat#35050–061
B-27 Plus supplement	ThermoFisher Scientific	A3582801
Neurobasal Plus	ThermoFisher Scientific	A35829–01
4% paraformaldehyde	ThermoFisher Scientific	J19943-K2
Triton-X	Sigma	9036–19-5
Bovine serum albumin	BioShop	Cat#1H72356
Vectashield	Vector Laboratories	H-1500
Critical commercial assays		
Fluo-4 Direct dye	Invitrogen	F10473
Coelenterazine H	Prolume	Cat#301–1 hCTZ
Coelenterazine 400a (Deep Blue C)	Prolume	Cat#340–1 CTZ 400a
Neurite Outgrowth Staining Kit	ThermoFisher Scientific	A15001
FD Rapid Golgi Stain Kit protocol	FD NeuroTechnologies, Inc	PK401
Geristore Syringeable Dual-Core Resin-Ionomer	DenMat	Cat#31458550
Nano-Glo(R) HiBiT Extracellular Detection System, 100mL	Promega	N2421
Experimental models: Cell lines		
HEK293T	ATCC	CRL-3216
Flp-In T-Rex 293 Cell Line	Invitrogen	R78007
Experimental models: Organisms/strains		
Sprague Dawley, IGS Rat	Charles River Laboratory	Cat#001CD
C57BL/6J	The Jackson Laboratory	Cat#000664
C57BL/6J	Charles River Laboratory	Cat#027CD
Recombinant DNA		
Aminergic GPCR Tango cDNA	Kroeze et al. 2015[108]	Addgene Cat#1000000068
pcDNA5/FRT/TO-Gq-Rluc8	Olsen et al. 2020[38]	Addgene Cat#140982
pcDNA5/FRT/TO -GoB-Rluc8	Olsen et al. 2020[38]	Addgene Cat#140977
pcDNA5/FRT/TO -Gs(short)-Rluc8	Olsen et al. 2020[38]	Addgene Cat#140980
pcDNA3.1-GFP^2-γ2	Olsen et al. 2020[38]	Addgene Cat#140989
pcDNA3.1- GFP^2-γ9	Olsen et al. 2020[38]	Addgene Cat#140991
pcDNA3.1- GFP^2-γ1	Olsen et al. 2020[38]	Addgene Cat#140989

REAGENT or RESOURCE	SOURCE	IDENTIFIER
pcDNA3.1-Gβ1	cDNA Resource Center	Cat#GNB0100000
pcDNA3.1-Gβ3	cDNA Resource Center	Cat#GNB0300000
Human-β-arrestin-2	cDNA Resource Center	Cat#ARRB200001
pcDNA3.1-GFP^2-human-β-arrestin-2	This paper	N/A
pcDNA3.1–5-HT1A-Rluc8	This paper	N/A
pcDNA3.1–5-HT1B-Rluc8	This paper	N/A
pcDNA3.1–5-HT1D-Rluc8	This paper	N/A
pcDNA3.1–5-HT1e-Rluc8	This paper	N/A
pcDNA3.1–5-HT1F-Rluc8	This paper	N/A
pcDNA3.1–5-HT2A-Rluc8	This paper	N/A
pcDNA3.1–5-HT2B-Rluc8	This paper	N/A
pcDNA3.1–5-HT2C (INI)-Rluc8	This paper	N/A
pcDNA3.1–5-HT4-Rluc8	This paper	N/A
pcDNA3.1–5-HT5a-Rluc8	This paper	N/A
pcDNA3.1–5-HT6-Rluc8	This paper	N/A
pcDNA3.1-human-GRK2	This paper	N/A
pcDNA3.1-HiBiT-5-HT2A	This paper	N/A
Software and algorithms		
Prism 9	GraphPad Software	Ver. 9.0.2
SPSS Statistics 26	IBM	Release 26.0.0.0
ChemDraw Professional 16.0	PerkinElmer	N/A
ChemStation Software	Agilent Technologies	G2170BA
AnyMaze	AnyMaze	Ver. 6.35
Deep Lab Cut (DLC)	Mathis Lab	Ver 2.2.1
Neurolucida 360	MBF Bioscience	Ver. 2021
Neurolucida Explorer	MBF Bioscience	Ver. 2021
Xen Black image analysis software	Zeiss	Ver. 2.1
Custom scripts for DLC/AnyMaze analysis	Andre Telfer	https://github.com/A-Telfer/bapipe-keypoints/tree/fd24e3c7b16bd9901db95f3bbc46efc6f13268f6
LabChart	ADInstruments	ver 8.0.2
Matlab	Mathworks	R2019a Update 4